A STUDY OF THE HYDROSTATIC AND HYDRODYNAMIC PROPERTIES OF *AEOLISCUS STRAIGATUS*

by

Jeremy Keifenheim

A Thesis Submitted in

Partial Fulfilment of the

Requirements for the Degree of

Master of Science

in Engineering

at

The University of Wisconsin – Milwaukee

May 2016

ABSTRACT

A STUDY OFTHE HYDROSTATIC AND HYDRODYNAMIC PROPERTIES OF *AEOLISCUS STRAIGATUS*

by

Jeremy Keifenheim

The University of Wisconsin-Milwaukee, 2016

Under the Supervision of Professor Thomas Consi

Aeoliscus strigatus is a highly maneuverable fish found in the Indo-Pacific region. It boasts a unique head down posture and employs median paired fin propulsion to perform precise movements. The need for highly maneuverable underwater AUVs for exploration and testing drove the examination of the hydrostatics and hydrodynamics influencing *Aeoliscus*. To determine the stability of *Aeoliscus* the center of gravity and buoyancy were found. Center of gravity was experimentally located using the three plumb line method while center of buoyancy was located using two separate methods. The first method utilized the measured buoyant force, a rigidly mounted fish and a tank of water raised to displace ½ of the buoyant force. Method two utilized a microcomputed tomography (micro-CT) system to create a 3D model of the fish and allowed for computational location of the center of buoyancy. The average normalized approximation of the center of gravity was found to be 0.46 posterior to the mouth and 0.34 ventral to the leading dorsal edge of the fish. The average normalized approximation of the center of buoyancy was found to be 0.46 and 0.45 posterior to the mouth and 0.35 and 0.43 ventral to the leading dorsal edge of the fish by the micro-CT system and the experimental method respectively. Velocity, Reynold's number and coefficient of drag were found to as a first step to understanding the hydrodynamics of *Aeoliscus*. The maximum observed velocity was 300 mm/s or about 22 body lengths per second, a Reynolds number of 4222, indicating laminar flow and a coefficient of drag of 0.029, which is similar to that of other fish.

TABLE OF CONTENTS

LIST OF FIGURES

LIST OF TABLES

ACKNOWLEDGEMENTS

The help, guidance and support of my colleagues, friends and family has been invaluable. Without this network surrounding me, I would not be where I am today. I would like to thank Will Mueller for beginning the work on *Aeoliscus*, Joseph Patzer for his suggestions and advice when finding the center of buoyancy, Dr. Ryo Amano for his insight into computational fluid dynamics and reviewing my thesis and Steve Houdek for his input, suggestions and the pain-staking task of reviewing all of my work.

Next I would like to thank Dr. Naira Campbell-Kyureghyan, Dr. Henry Tomasiewicz, and Blake Johnson for the exuberant amount of time they spent helping me learn a system and software that were vital to my project. Without their guidance I would not have been able to maintain the crucial time line I was committed to. I would also like to thank Dr. J. Rudi Stickler for more things than I can list. His advice, knowledge of imaging methods and the occasional nudge in the right direction were invaluable.

I would like to express my gratitude to my advisor, Dr. Thomas Consi. Over the past two years of my life Dr. Consi was always available to discuss ideas, perform experiments, develop methods and review results. His time and resources commitment was enormous and he went above and beyond what any advisor should ever have to do. I enrolled in a class taught by Dr. Consi during my final year of my undergraduate work and, while I was on the path to graduate school, I had decided to end my schooling after the completion of my bachelor's degree. His interest in me and encouragement was the only reason I chose to continue. I can truly say I would not be where I am today if it had not been for Dr. Consi.

Finally I would like to thank my wife. Her help and understanding when classes became difficult and my work interfered with our lives made everything possible. None of this would have possible without her love and support.

Chapter 1: *Aeoliscus strigatus* Overview and Motivation

Examining the solutions of the past has long been a source of inspiration for engineers. Reviewing previous engineering designs, both within and outside of, the current discipline has led to solutions to current problems. Increasingly complex problems drives the need to be more innovative and creative and has driven engineers and designers to not only examine man-made solutions but also those that exist in nature. Merriam-Webster defines biomimetics (or biomimicry) as "the study of biological mechanisms and processes especially for the purpose of synthesizing similar products by artificial mechanisms which mimic natural ones." [1] This thesis is inspired by the need for small, highly maneuverable autonomous underwater vehicles (AUVs) for exploration inspection applications and as previous engineers have done, Mother Nature was consulted for inspiration. One particular fish, *Aeoliscus strigatus*, possesses a set of characteristics uniquely fit for exploration and inspection within tight geometrical constraints.

Aeoliscus strigatus, more commonly known as the shrimpfish, is a unique and highly maneuverable fish found in the Indo-Pacific region. Typically found within coral reefs and grass beds [2], it boasts an unusual head-down vertical orientation and combines that unique posture with powerful pectoral fins to perform a variety of precise movements. Along with basic horizontal and vertical translation, the shrimpfish can perform more advanced movements such as inserting itself between the spines of a sea urchin [2], turning in place, hovering and assuming a horizontal posture for fast swimming (mouth forward). Usually found in large schools, the school is capable of turning their narrow edges toward predators in unison to avoid detection.

Aeoliscus strigatus, shown in figure 1.1, is a rigid-body fish that resembles the physical traits of a straight razor. Adult fish can reach a length of 20 cm (anterior to posterior) while being only a few millimeters wide (left to right). The body is at its widest point near the dorsal side of the fish and gradually

diminishes as you approach its ventral side. The depth (dorsal to ventral) of an adult fish is around 13 mm. The dorsal to ventral width and anterior to posterior length aspect ratio at its widest point is on the order of 10^{-1}. These physical characteristics have earned the shrimpfish the nickname “razorfish.” At the most posterior end of the fish, is a hinged tail spike. Anterior to the tail spike and located on the ventral side of the fish is a set of three fins comprised of the anal, caudal and dorsal fins. Further anterior are the slender, paired ventral fins. The ventral fin consists of only a few fin rays each and their impact on propulsion is not clear. Anterior to the ventral fin is a pair of large pectoral fins, pair of gills and pair of eyes. At the most anterior part of the fish is long, tubular snout that terminates with a small trap-door-like mouth. This trap-door-like mouth, combined with the hinge located at the base of the snout allows the shrimpfish to quickly suck in small crustaceans from the water column.

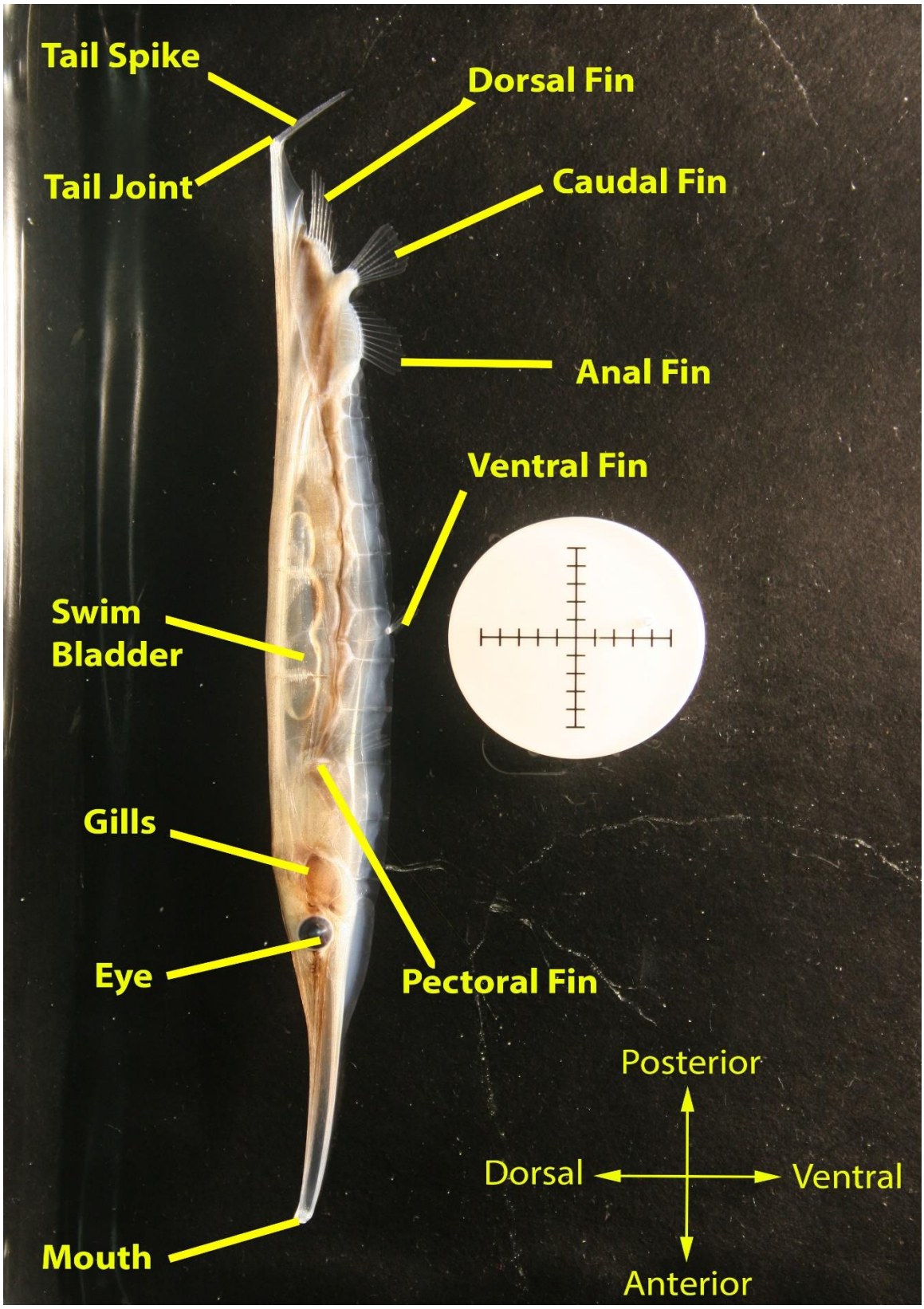

Figure 1.1: The shrimpfish, Aeoliscus strigatus in its normal head-down swimming posture. Scale is 2 cm in both directions, small division = 2 mm.

Aeoliscus boasts the ability to swim not only in its usual vertical orientation but also in a horizontal, mouth forward orientation. To achieve such motion, varying fin kinematics must be employed and a review of the terminology of biological fin breakdown is required. Paired fins are fins that are located on either side of the body. They are the pectoral and pelvic (ventral) fins which are supported, respectively, by the pectoral and pelvic girdles of the fish. Median or unpaired fins that are those in line with the axial skeleton and supported by the median elements associated with the vertebral column. They are the dorsal fins that run along the back, the caudal (tail) fin and the anal fin located ventrally just behind the anus of most fishes. [3] In *Aeoliscus* the orientation of the fish is rotated 90° and the dorsal fin has migrated to the posterior-ventral side.

Motion while in the vertical orientation was observed as two separate functions, turning and forward motion. Turning was observed from the posterior of the fish while forward motion was observed from multiple orientations. *Aeoliscus* displayed the ability to turn in place by utilizing its pectoral fins to create a moment about its spine while the caudal, anal and dorsal fins apparently act primarily as a rudder. The posterior three fins do show complex motion patterns so they probably generate thrust as well. *Aeoliscus* employs median-paired fin (MPF) [4] swimming as its primary method of locomotion. The velocity of forward motion will be presented in the following chapters.

The fins of Aeoliscus are transparent, in constant motion and are very difficult to observe in freely-moving fish. The detailed kinematics of *Aeoliscus* fins will, therefore, be the subject of a later investigation.

Chapter 2: Hydrostatics and Stability

2.a: Introduction

Merriam-Webster defines stability as "the property of a body that causes it, when disturbed from a condition of equilibrium or steady motion, to develop forces or moments that restore the original condition." [1] Examining a body and assuming there is a small force that changes the body's position, three things can occur. The body returns to its initial position; we say that the body is stable. The position of the body continues to change; we say in this case the body is unstable. In practical terms this can mean, for example, that the floating body capsizes. Finally the body remains in the displaced position until the smallest perturbation causes it to return to initial position or to continue to move away from the initial position. We call this situation neutral equilibrium where the sum on all moments (M) are zero. [5]

$$\sum M = 0 \qquad (2.\ 1)$$

The two factors that influence the stability of an object that is either partially or completely submerged are buoyant and gravitational forces; these two forces define an objects equilibrium position. Archimedes' principle defines the buoyant force as the weight of the fluid a body displaces [6] and gravitational forces (weight) is defined as the mass of the object multiplied by the force of gravity. [7] When examining these forces and their effects on an object's equilibrium, the need to apply the calculated forces at specific points becomes apparent. The center of gravity (CG) is the average position of the weight distribution of an object (or group of objects). [7] It is the point through which the weight of a body, or collection of bodies, may be considered to act. An object's CG is determined by the shape

of the object, the distribution and density of the materials in the body, and gravity. [7] For *Aeoliscus,* varying densities of bone and soft tissue could potentially cause the CG to be separate from the centroid of *Aeoliscus's* shape, which creates the need for a method to determine the CG separately from volume calculations.

2.b: Experimental Methods and Results

To experimentally determine the center of gravity, we utilized the plumb line method for 2D CG localization. [8] The fish was suspended in air on a freely rotating pivot and allowed to find its equilibrium position. A picture was then taken and a plumb line digitally added to the image using Adobe Photoshop. To ensure a true (parallel to the force of gravity) plumb line was digitally drawn, a physical plumb line was included in the field of view when the image was taken. The physical line was then traced and transferred so the line intersected the suspension point of the fish. The process was repeated for three unique suspension points and the images were layered and rotated until the images of the fish bodies were superimposed. This resulted in an image of *Aeoliscus* with three lines crossing at a single point within its body. The intersection of the 3 plumb lines is the center of gravity in the plane of which the image was taken. Because the fish is symmetrical about a median plane, we can assume the center of gravity lies on that plane. A step-by-step procedure is listed after the center of buoyancy review.

The center of buoyancy (CB) is the point through which buoyant force acts and it corresponds with center of gravity of a body with uniform density. The buoyant force is the density of displaced fluid (ρ) multiplied by the volume (V) of the displaced fluid and is independent of the distribution of mass within the submerged body. Mathematically the buoyant force is as follows. *[6]*

$$F_B = \sum \rho g V \qquad (2.2)$$

Two different methods of calculating CB were utilized. The first was an experimental method that involved securing a euthanized fish and lowering it into water until ½ of the measured buoyant force was displaced (full method listed below) while the second involved the use of a Micro-CT system and software to the calculate the CG of a 3D model of *Aeoliscus* with uniform density. The location of both the CG and CB were then compared. The vertical distance between the CG and CB is known as the metacentric height. *[5]*

When developing the optimal method for both the CG and CB calculation, six fish were sacrificed to perfect the method. We began by euthanizing a fish using ½ gram of tricaine methanesulfonate (MS-222) dissolved in 1 liter of seawater. After insuring all gill movement had ceased, *Aeoliscus* was left in the solution for 5 minutes to ensure death. After the waiting period had passed some initial length measurements were taken.

The measurements for five fish experimented on after the method was optimized are shown in table 2.1. The standard length (Table 2.1) of the shrimpfish was measured from the tip of the mouth to the joint of the tail spike using a Mitutoyo digital caliper (Mitutoyo Aurora, Illinois). This measurement was chosen because the tail spike was frequently broken or in various states of regeneration. The distance from the tip of the mouth to the base of the pectoral fin was also measured (Pec Fin Base, Table 2.1). The maximum dorsal to ventral depth (Depth, Table 2.1) of the fish was measured at the level of the pectoral fins. The maximum width of the fish (dorsal to ventral dimension, Width, Table 2.1) was measured at the level of the gills (the widest part of the fish).

Mass (M_g) was defined to be the mass of the fish out of water with external water removed but with its internal water retained (Wet Mass, Table 2.1). Internal water included the water in the tubular mouth and the gills. To measure mass, a euthanized shrimpfish was held by the thumb and forefinger and shaken 3 times to remove the external water. It was then placed in a dry, tared weighting boat and

weighed on a digital balance (Adventurer Pro AV213, Ohaus, Parsippany, NJ) with a resolution of .001g and a linearity of .002g. The mass measurements were made assuming that the buoyancy of air was negligible.

The mass of the water displaced by the shrimpfish, M_d (Displacement, Table 2.1) was measured as follows. A vertically-mounted glass tube with a fine horizontal line (part of its trademark symbol) was filled with seawater to the level of the line (bottom of the meniscus tangential to the line). The line and water level were observed with a low-power, horizontally mounted microscope. The euthanized fish was placed in the tube, completely submerging it, and the water was carefully removed to the level of the horizontal line. The removed (displaced) water was weighed on the same digital scale as was used for the wet mass measurement. This method automatically accounts for the density of the seawater. Since g is a constant we found it convenient to use mass as a surrogate for force, thus the "force of gravity" corresponds to M_g and the "buoyant force" corresponds to M_d. The net buoyancy (M_{bnet}) is simply the difference between the mass (M_g) of the fish and the water displacement mass (M_d). Buoyancy was also expressed as a percent of the wet mass (last column, Table 2.1).

$$M_{b,net} = M_B - M_g \qquad (2.3)$$

Fish	Standard Length (mm)	Pec Fin Base (mm)	Depth (mm)	Width (mm)	Wet Mass (g)	Displacement (g seawater)	Net Buoyancy (g)	Buoyancy as % of mass
7	116.9	48.4	13.4	3.7	1.582	1.514	-0.068	-4.49
8	117.7	50.1	12.8	3.3	1.543	1.484	-0.059	-3.98
9	127.8	52.8	13.7	4	2.178	2.037	-0.141	-6.92
10	125.8	52.2	13.4	3.7	1.995	1.885	-0.11	-5.84
11	114.4	49.5	12.8	3.8	1.528	1.326	-0.202	-15.23

Table 2.1: Dimensions, mass and buoyancy measurements of five shrimpfish.

The center of gravity was determined using the three plumb line method. To begin a plumb line was set up using fishing line with a weight attached to the end. The weight was placed in a beaker of water to

dampen the vibration of the building. Along with the plumb line, a 2 cm scale was placed. All three objects were placed in the same plane of focus Next the Photonfocus camera (Photonfocus, Lachen, Switzerland) was set up to image the fish, scale and plumb line.

The euthanized shrimpfish was removed from the seawater and shaken 3 times to remove residual water. Using a pin, *Aeoliscus* was impaled with the spine towards the posterior end of the fish (same orientation as figure 1.1), ensuring that the fish could rotate freely about the pin. The fish was then spun and allowed to find its equilibrium point and an image was captured. The fish was then removed from the pin and impaled in a difference location. The process was repeated 3 times with three different pin insertion points. After the images were acquired, each was brought into Adobe Photoshop (Adobe San Jose, CA). Using Photoshop, the plumb line was traced and the trace was adjusted to fall over the insertion point of the pin. The three images were then overlaid and adjusted so that the fish bodies were superimposed on each other. This procedure determined the location of the center of gravity in the antero-posterior direction measured from the tip of the mouth (CG, A-P, Table 2.2) and dorsal-ventral direction measured from the dorsal side (CG, D-V, Table 2.2). These distances were normalized to the standard length (Norm. CG, A-P), and to the depth of the fish (Norm. CG, D-V, Table 2.2).

Next we examined the center of buoyancy utilizing the same digital scale, camera set up and 2cm scale previously mentioned. To begin, *Aeoliscus* was secured to a small plastic card using cyanoacrylate glue. The digital scale was placed on a raised platform. The water tank was filled with seawater and placed on a vertically adjustable lifting platform below the scale and a suspension apparatus was attached to the digital scale (Fig. 2.1). This apparatus allowed us to attached *Aeoliscus* to the scale via a bolt. *Aeoliscus* was attached to the apparatus and the digital scale was zeroed. Once the scale was ready, the lifting platform was used to raise the water tank until ½ of the buoyant force of the fish was displayed (Fig. 2.1). At this point, the camera's vertical position was adjusted to ensure it was level with the water and an image was taken. The process was repeated three times, each time adjusting the angle of the fish

utilizing the rotational joint allowed by the bolt. Using Photoshop, a horizontal line was traced at the water level for each image and the images were overlaid and adjusted. The intersection of the three lines was the center of buoyancy.

The procedure determined the location of the center of buoyancy in the antero-posterior direction measured from the tip of the mouth (CB, A-P, Table 2.2) and dorsal-ventral direction measured from the dorsal side (CB, D-V, Table 2.2). These distances were normalized to the standard length (Norm. CB, A-P), and to the depth of the fish (Norm. CB, D-V, Table 2.2).

Fish	Std. Length (mm)	Depth (mm)	CG, A-P (mm)	Norm. CG, A-P	CG, D-V (mm)	Norm. CG, D-V	CB, A-P (mm)	Norm. CB, A-P	CB, D-V (mm)	Norm. CB, D-V
7	116.9	13.4	51.3	0.439	4.51	0.337	49.9	0.427	5.33	0.398
8	117.7	12.8	55.6	0.472	4.21	0.329	53.2	0.452	5.52	0.431
9	127.8	13.7	59	0.462	4.94	0.361	57	0.446	5.76	0.420
10	125.8	13.4	58.7	0.467	4.65	0.347	56.7	0.451	5.73	0.428
11	114.4	12.8	54.3	0.475	4.45	0.348	53.2	0.465	6.12	0.478

Table 2.2: Locations of the center of gravity (CG) and center of buoyancy (CB).

One crucial alteration to the seawater that was used during the CB experimental measurement, was the addition of a surfactant. Surfactants reduce the interfacial tension between two unique surfaces. When initially performing the CB measurement, no surfactant was used and a large meniscus was observed between the fish and the water. This meniscus pulled the fish in a downward direction effectively adding to its weight. This resulted in a CB line that was higher (toward the suspension point) than the true line. Reducing the surface tension with a surfactant greatly reduced this source of error in the measurement. The surfactant used was BRIJ-35 (Ricca Chemical Company, Pocomoke City, MD) at a concentration of 1 mL surfactant to 16 L seawater. To observe the effect of the surfactant, a control stick with similar surface area to *Aeoliscus* and of uniform density was machined and the CB was experimentally determined and compared with the geometrically determined CB. A rectangular shape was used for the control stick as it allowed for easy CG and CB mathematical geometry based calculation. We found that

the surfactant greatly reduced the interfacial tension. We observed a residual error of about 1% (both n the dorsal-ventral and the anterior-posterior directions) and those factors were used to adjust the experimental CB results. Table 2.3 below shows the measured CB of the control stick with and without surfactant using the same apparatus and procedure used with the fish. The two different control stick CB overlays can be seen in appendix B. Table 2.3 below offers the surfactant control measurements and calculations. As a rectangular stick was used, the CB should be located at a normalization of 0.500 in both A-P and D-V directions. Figure 2.2 shows the location of the CG, CB and surfactant-adjusted CB (labeled as corrected CB) on the shrimpfish. Images showing the individual CG and CB images along with the overlaid fish specific CG/CB locations can be seen in appendix A.

	CB, D-V (mm)	**Norm. CB, D-V**	**CB, A-P (mm)**	**Norm. CB, D-V**
Control w/surfactant	37.600	0.493	6.13	0.499
Control w/o surfactant	36.770	0.483	6.13	0.499

Table 2.3: Control stick CB measurements.

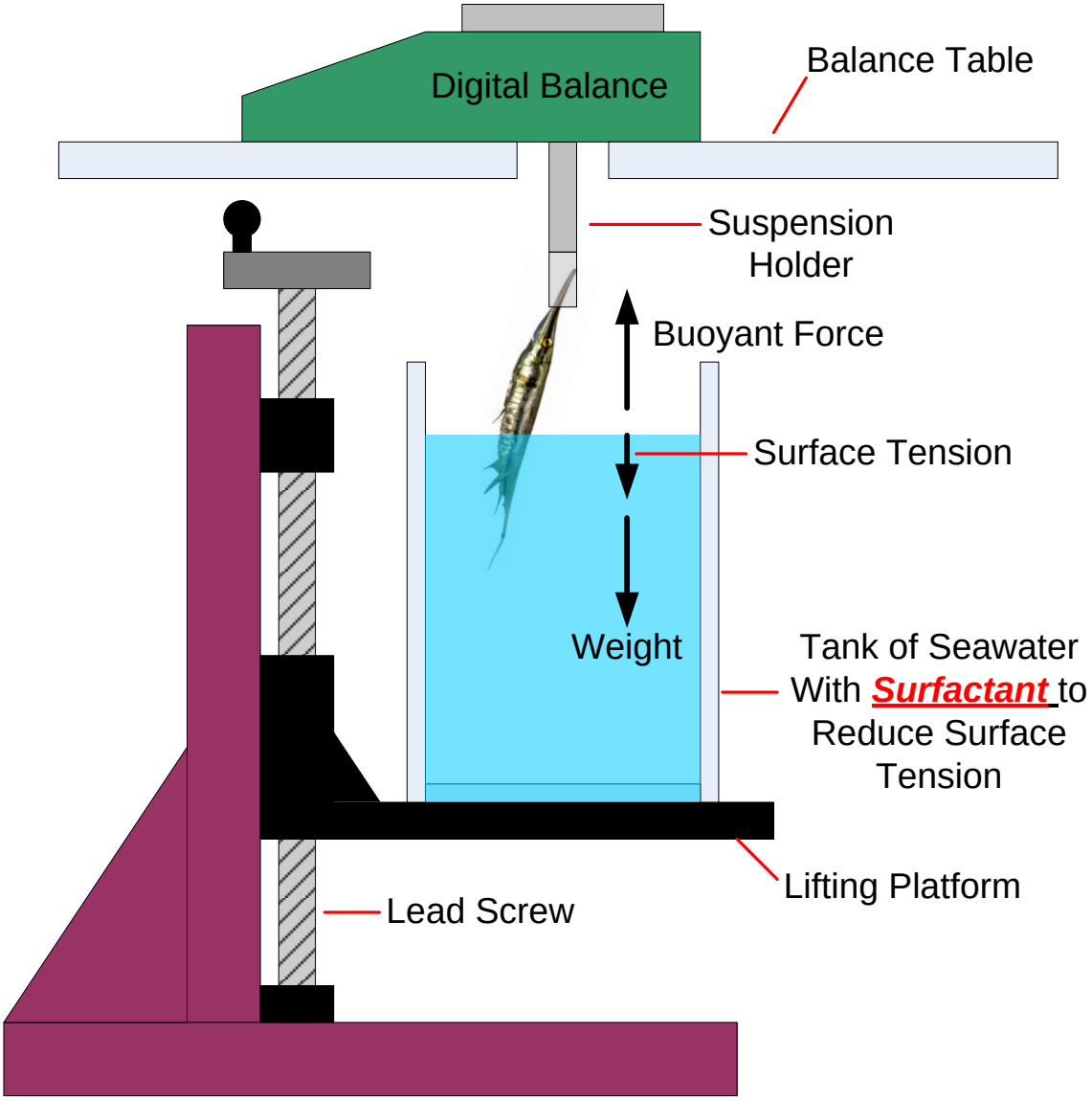

Figure 2.1: Center of buoyancy measurement apparatus, see text for details.

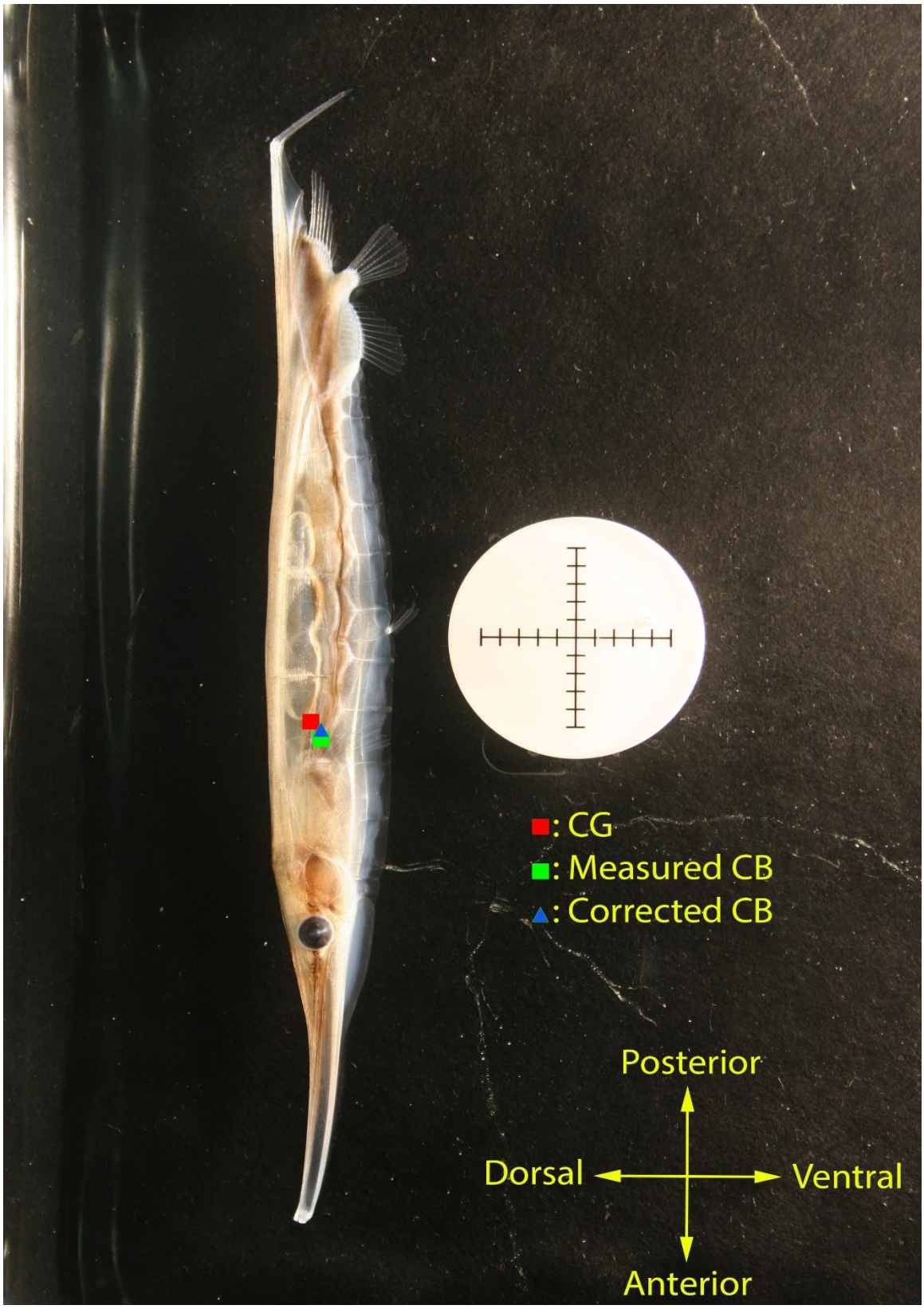

Figure 2.2: Aeoliscus with labeled experimental CG and CB. Scale is 2x2 cm with smallest division of 2 mm.

2.c: MicroComputed Tomography

An additional method to calculate the center of buoyancy of an object with non-uniform density, is to create a 3D model of the object with a material of uniform density. For an object of uniform material, the center of buoyancy and the center of gravity are coincident. There are two different methods to generate a 3D model, physically or mathematically using computer software. Each method brings to the table different concerns and issues.

One of the most considered methods to physically model an object of unique shape is to create a mold of the object and produce a cast replica made of uniform material. *Aeoliscus's* small and intricate profile create difficulties in both creating the mold and then casting the part. Small details and thin cross-sections will be obscured or even lost completely. Mathematically calculated (computer) models also present challenges. Before a model can be created, it must first have a 3D scan of the object. The more traditional method of utilizing an optical 3D scanner to obtain an exterior profile of *Aeoliscus* is not ideal. In order to adequately maintain the soft tissue, the tissue must be kept hydrated. As water is naturally reflective, it creates variability in the density of the reflected laser causing errors in the resulting 3-D reconstruction. One method that allows for the hydration of the soft tissue and still allows for a 3D exterior profile to be created is the use of low-powered x-ray micro-computed tomography (micro-CT). Micro-computed tomography, micro-CT for short, is a high resolution x-ray CT. X-ray CT is a noninvasive and nondestructive imaging method where individual radiographs that are recorded from different viewing angles are utilized to reconstruct the 3D structure of an object. Micro-CT systems are similar to medical CT systems but offer higher resolution and are used primarily by researchers. [9] When utilizing x-ray CT technology, the visibility of an animal's tissue depend on its contrast relative to its surroundings and its spatial resolution. The brightness of an animal's tissue is determined by the degree of its ability to absorb the x-ray. [9] Bone, for example, absorbs X-rays much better than muscle or other soft tissues thus conventional X-ray images show primarily bone. Staining soft tissues with a contrast enhancement

agent such as iodine, will enable them to better absorb x-rays and thus show as brighter images in the radiograph (x-ray image). The better a material's ability to absorb, the higher its grey level value where grey level is defined as the brightness of a pixel. When examining biological material, different tissues (such as bone, cartilage and muscle) have different x-ray absorption abilities and therefore show as different grey level values in the radiograph. Because we are using settings that allow us to capture the exterior of the fish (discussed later), the contrast between the fish and air is high. Combined with the high spatial resolution of the Micro-CT system used, the exterior details of the fish are clear.

The micro-CT system used was a Zeiss Xradia 410 Versa (Carl Zeiss X-Ray Microscopy, Pleasanton, CA) with a spatial resolution of 0.9 micrometers and minimum voxel (volume element) size of 100 nanometers. Our 410 Versa model was the high energy model, where the voltage and power ratings are 40-150kV and up to 10W respectively. [10] In order to capture the exterior shape of the fish, which includes both bone and soft tissue (skin), the power settings and voltages had to be lowered to 6W and 40kV and an x-ray filter to block specific wavelengths was implemented. Varying scan areas and resolutions can be obtained using different objective lenses and scans per revolution respectively. Reducing the power and voltage allows for a lower contrast differential between the varying tissues and allows for the imaging of the soft tissue and bone exterior.

Creating a 3D profile of an object using a micro-CT system involves two separate processes: imaging and reconstruction. The visibility of an object's individual components depend on its contrast relative to its surroundings and the spatial resolution of the micro-CT system. [9] After image acquisition has been completed, reconstruction from x-ray projections can be performed using multiple methods and varying mathematical models. Only that of which the Xradia 410 Versa uses, absorption contrast, is discussed. Absorption tomography measures the linear absorption coefficient of each ray through the object. The linear absorption coefficient is the attenuation of all local absorption coefficients where each local coefficient can be approximated for each voxel. Approximating the local coefficients is the pivotal

problem associated with computer tomography and is overcome by taking absorption measurements at many ray directions. In order to examine this process mathematically, we must look at the equation for the attenuation of x-rays of a given wavelength, λ, through homogenous material developed by Rontgen. [9]

The intensity of a beam after passing through a material is given by equation 2.4 below.

$$I = I_o \, exp(-\mu x) \qquad (2.4)$$

I_o is the unattenuated beam intensity, μ is the material-specific linear attenuation coefficient and x is material thickness. We can rewrite equation 2.4 as

$$I = I_o \, exp((-\mu/\rho)\rho x) \qquad (2.5)$$

where μ/ρ is the mass attenuation coefficient and ρ is the density. Given a ray **s**, we can look at each individual voxel and linear attenuation coefficient. To do this we need to examine the attenuation for small thickness elements (dx). Equation 2.6 below gives the change in intensity per change in distance

$$\frac{dI}{I_0} = -(\mu/\rho)\rho \, dx \qquad (2.6)$$

where dx is dependent on the micro-CT system being used. Introducing ray **s** into equation 2.6 yields

$$I = I_o \, exp(-\int \mu(s) \, d\boldsymbol{s}) \qquad (2.7)$$

Rearranging equation 2.7 yields

$$\int \mu(s) \, d\boldsymbol{s} = \ ln(\frac{I}{I_o}) \qquad (2.8)$$

$\frac{I}{I_0}$ is precisely measured for many different position for each ray **s** and when combined with the many different directional angles, a 3D reconstruction can be obtained. *[9]*

The Xradia 410 was used to scan 4 separate fish that were sacrificed in MS-222 and preserved in 10% neutral-buffered formalin. Note that the four fish used in the micro-CT measurements were not the same fish as used in the experimental measurements for CG and CB (section 2.b). Prior to scanning, each fish was rinsed in deionized water and then immersed in 100% Lugol's solution and allowed to absorb the stain for 1 to 3 days. Lugol's solution is a combination of iodine and potassium iodide and was used to increase the x-ray absorption of the soft tissue on the ventral side of the fish, the bony dorsal side readily showed in the images without staining. The clarity of the scans did not appear to be affected by the amount of time the fish was immersed in the solution. After removal from the solution each fish was rinsed with de-ionized water and sealed in a plastic test tube to prevent evaporation and keep the soft tissue humidified. Due to the magnification and length of the fish multiple scans had to be taken, at different points along the fish. The multiple scans were then stitched together to give the complete profile of the fish. Each individual scan consisted of 800 individual 2D x-ray images taken every 0.45^{o}.

Post-processing of each stitched scan was done in multiple steps. First the file must go through a type conversion. This is done using a GUI developed for Matlab (Mathworks, Natick, MA) known as TXM Wizard. TWM Wizard converts various input file types to various output file types. [11] The Xradia 410 system outputs a stitched file of type txm. The file is then converted and separated into jpeg files, each of a single 2D x-ray image that can be brought into the next step of post-processing. Step two is the process of eliminating unwanted materials by contrast. Contrast is broken down into a range of grey values; the higher the grey value, the higher the x-ray absorption of the material. A grey value of zero corresponds with a pixel with no brightness (black) up to pixel of full brightness (white). The images are then brought into the Mimics (Materialise, NV, Belgium) software. Mimics allows the user to alter each image based on grey value ranges, manual editing, cropping and a host of other methods. When the user is satisfied that all undesirable material has been removed from the images, Mimics can be used to

generate a 3D profile. At this stage we leave the Mimics software to utilize another software program developed by Materialise, 3-Matic.

3-Matic is a three-dimensional modelling program, similar to those commonly used in the field of structural and mechanical engineering but is focused more on processing unique objects not normally seen by mechanical or structural engineers. Through 3-Matic, smooth models were generated and the center of gravity was found. 3-Matic offers various methods to calculate the center of gravity; as we are using the volume of the fish to calculate the CB, the method used in 3-Matic was the center of volume. When importing from Mimics to 3-Matic, the model scales but does not maintain the appropriate dimensions. Because the CG and CB were normalized when determined experimentally, the scaled unit was not an issue. Table 2.4 below shows the results from 3-Matic. It should be noted, as previously discussed, that the CG of an object constructed of a material of uniform density is coincident with that objects CB, whether the object is of uniform density or not.

Fish	Overall length	A-P Distance	Norm. A-P	Overall Width	D-V Distance	Norm D-V
1	3179.39	1477.2	0.465	356.54	126.17	0.354
2	3381.03	1525.87	0.451	336.52	118.74	0.353
3	2675.82	1161.12	0.434	295.14	95.7	0.324
4	3364.87	1609.63	0.478	413.92	155.87	0.377
Average	3150.278	1443.455	0.457	350.530	124.120	0.352

Table 2.4: 3-Matic CG Measurements

Finally the normalized averages were put into table 2.5 below for a numerical comparions with the experimental data. While there is not method to calculate the CG using the micro-CT method we utilized the data was left in for comparison. The data shows that a normalized A-P CB for the experimental method and the micro-CT method were within 1% of each other. There was an 8% difference between the experimentally determined D-V CB and the micro-ct calculated D-V CB. Figure 2.3 shows the location of the calculated CG and CB measurements.

	Norm. A-P CG	Norm. D-V CG	Norm. A-P CB	Norm. D-V CB
Experimental Average	0.463	0.344	0.448	0.431
Micro-CT Average	NA	NA	0.457	0.352

Table 2.5: Comparison of averaged normalized CG and CB measurements from experimental data and micro-CT data.

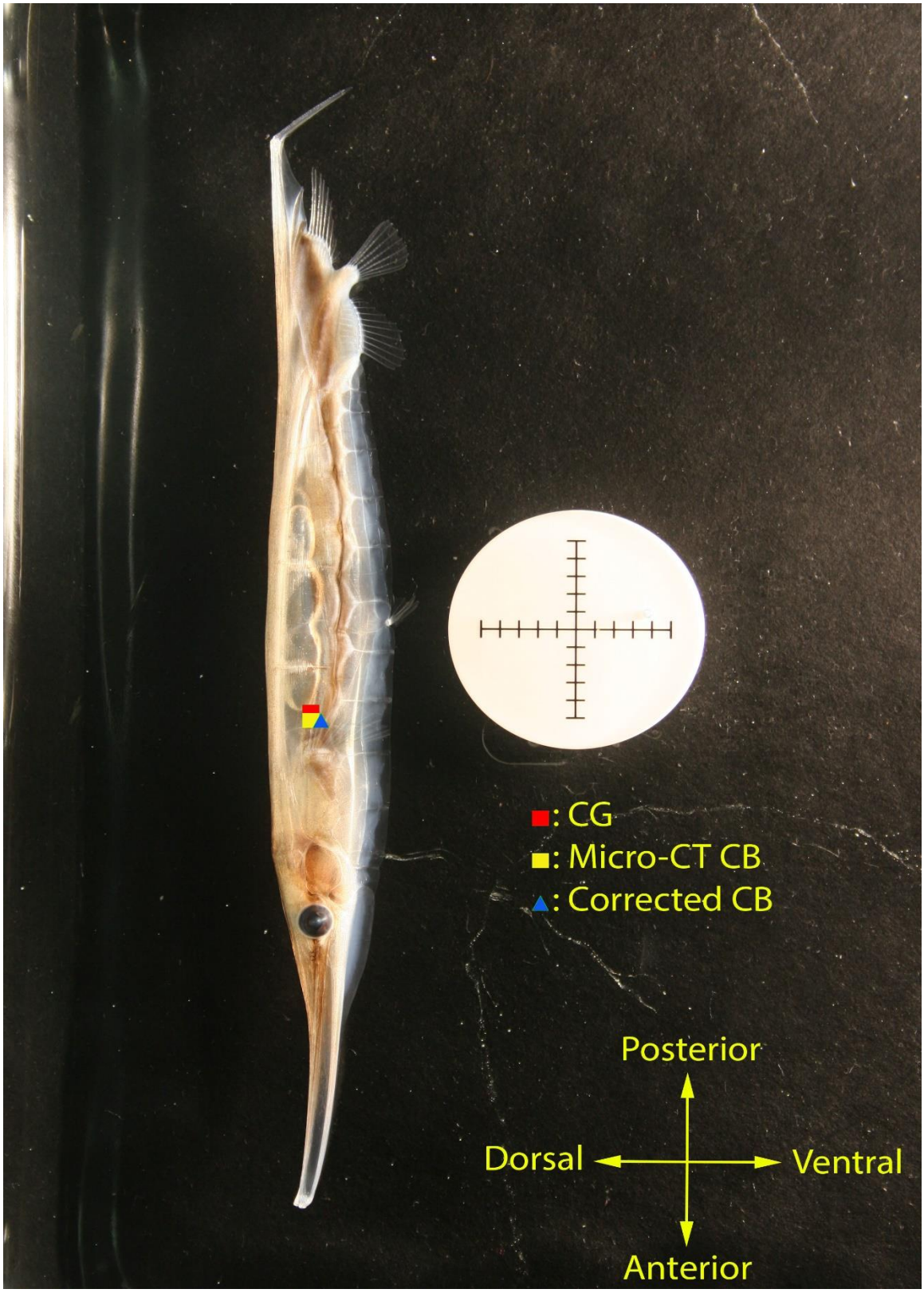

Figure 2.3: Comparison of Micro-CT generated CB, and the experimentally measured CB and CG. Corrected CB took into account the surface tension force that existed in our CB measurement technique. See text for details.

Chapter 3: Hydrodynamics and Maneuverability

Hydrodynamics, as defined by Merriam-Webster, is "a branch of physics that deals with the motion of fluids and the forces acting on solid bodies immersed in fluids and in motion relative to them." [1] When examining objects moving through a fluid the drag force is one of many highly influential forces. As we are currently only interested in the drag force, only it will be discussed. Drag force directly influences the amount of energy needed to move the object through the fluid. For self-propelled organisms such as fish a lower drag force makes swimming and maneuvering more efficient. .

3.a: Maneuverability

To quantify the maneuverability, the definition established by Norber and Raynor [12], and later accepted by Webb [13]was adopted. Norber and Raynor defined maneuverability as the ability to turn in a confined space and they utilized the length-specific minimum radius of the turning path (r_{path}/L, where L is total body length) to measure and compare between swimming animals.

To observe the maneuverability of the shrimpfish a video camera was set up above a viewing tank to observe the turning radius. The fish was recorded using the same Photonfocus camera and Fujinon lens as the still images used for the hydrostatics using a 10 ms exposure at 60 FPS. The software used to capture the video was Streampix 6 (Norpix, Quebec, Canada). The video was converted to individual frames and exported using Adobe Photoshop. A line was drawn from the dorsal to ventral side of the fish and the images were overlaid, similar to the process done when determining the CG and CB. Figure 3.1 below shows the overlaid images. While only 5 images have been used, they span ¼ second. As you can see, the lines intersect at a common point. *Aeoliscus* can turn on axis and is therefore highly maneuverable. The overlay shows that within that ¼ second, *Aeoliscus* rotated 90^{o} demonstrating that it can turn at a rate of at least 1 revolution per second.

Figure 3.1: Turning Radius Overlay

3.b: Coefficient of Drag

The next dynamic property we examined was the coefficient of drag (C_D). The coefficient of drag is a non-dimensional parameter that relates the drag an object to the area over which the force occurs and at the velocity at which the force occurs. Equation 3.1 below mathematically defines the C_D

$$C_D = F_D / (\frac{1}{2}\rho V^2 A) \quad (3.1)$$

where F_D is the drag force, ρ is the density of the fluid, V is the velocity and A is the characteristic area. [6] The C_D is also the sum of the of two individual coefficients of drag, that due to the pressure differences surrounding the fish and that of the friction due to the surrounding fluid's resistance to shear. [6]

The coefficient of drag can be either experimentally measured or estimated using current computational fluid dynamics (CFD). Due to the difficulties involved in experimental methods coupled with the fact that we already have a 3D model of the fish we chose to use CFD. Before we can utilize CFD we needed to determine both the velocity and Reynolds number, starting with velocity. While *Aeoliscus* can swim in both a horizontal and vertical orientation, only the vertical forward motion was measured. To measure velocity a 24 3/8" x 6" x 8" tank with a white background was filled with 4 gallons of seawater. The same camera/lens setup as the turning observation was used with Streampix once again capturing the frames. *Aeoliscus* was placed in the tank and encouraged to move using a glass stirring rod.

Post-processing once again involved multiple steps. First the video was imported into Maxtraq 2D (Innovision Systems, Columbiaville, MI). Maxtraq 2D allows of two dimensional position tracking between frames and includes the option to set a custom scale. This data can then be examined using additional Maxtraq software or exported to be processed using other software. To process our data, the x-y location information was imported into Matlab. A custom Matlab script was written that takes the frame rate, the x-y data file and the desired output file name and creates an x-position vs time graph, y-position vs time graph and text file with the maximum unit-less velocity. The Matlab script can be reviewed in the appendix. Four fish were observed and processed; the maximum calculated velocity was 300 mm/s. To observe the most extreme case, 300 mm/s will be used to calculate the C_D. The position tracking can be seen in figure 3.2 below.

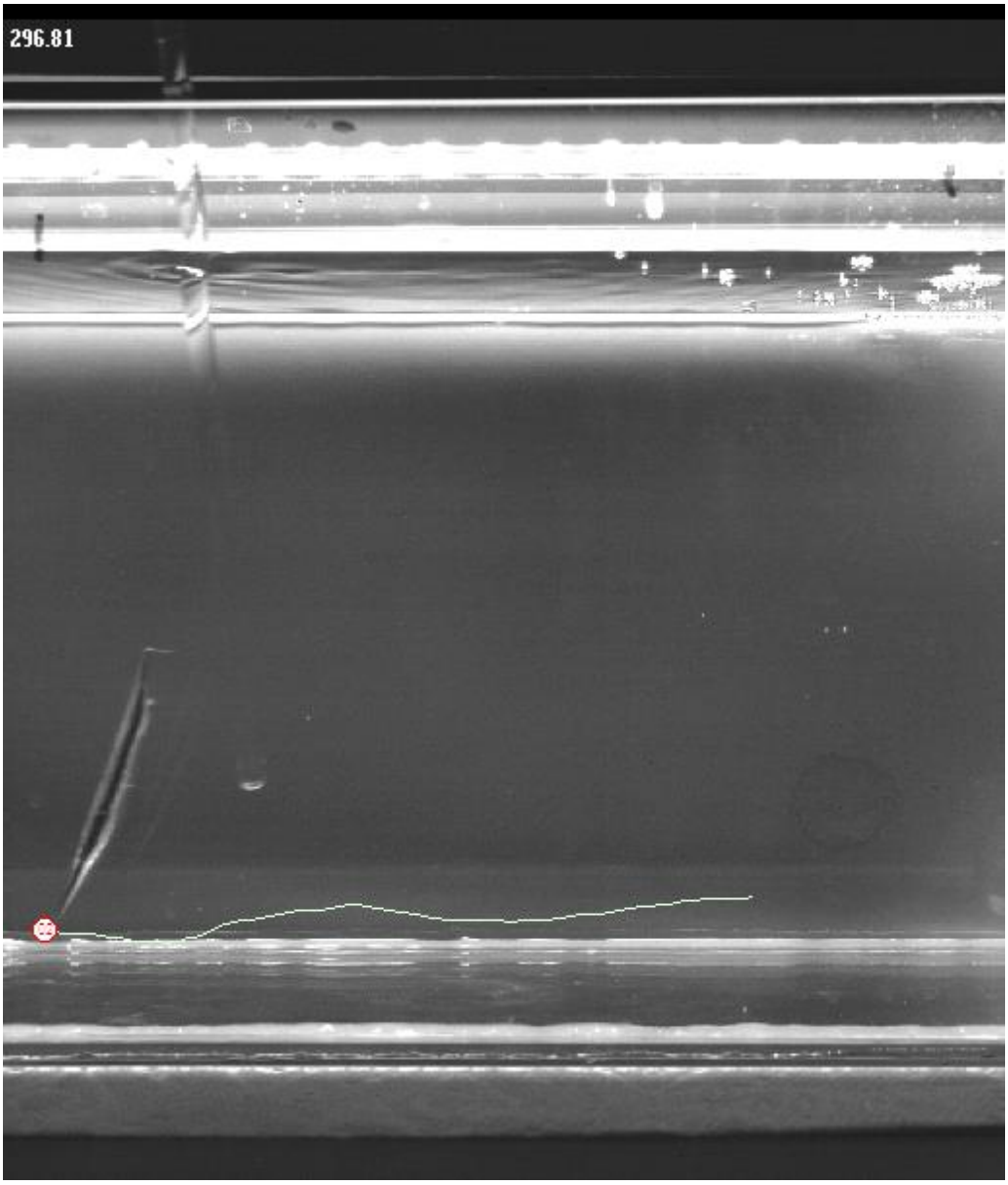

Figure 3.2: Maxtraq processed fish track

Now that we have a maximum velocity we can examine the Reynolds number (Re). The Reynolds number is a dimensionless parameter correlating the viscous behavior of all Newtonian fluids. Equation 3.2 shows the mathematical model of the Reynolds number

$$Re = \frac{\rho V L_c}{\mu} \quad (3.1)$$

where L_c is the characteristic length, V is the velocity and μ is the viscosity. As the fish cross-section resembles that of an airfoil, the characteristic length used was the chord length (depth measurement of the fish). Using density and viscosity for seawater at 25^{o}C and a salinity of 33 ppm, the resultant Reynolds number of 4222. According to White [6], Reynolds numbers on the order of 10^6 are on the lower border of turbulent. As our data shows a laminar flow around the fish, a laminar flow model must be used.

To model the flow around *Aeoliscus*, Ansys Workbench (ANSYS, Inc. Canonsburg, PA) was coupled with another Ansys package, Fluent. To model a fluid flow, the fluid itself must be created. For an external flow, the geometry around which you wish to model the flow must be removed from a surrounding fluid volume. To do this another 3D modeling program, Autodesk Inventor (Autodesk, Inc. San Rafael, CA), was used. Using Inventor a thin cross-section fluid volume was created and centered 1 mm posterior to the pectoral fin base. This allows for the capture of the maximum width and depth of the fish without including the partially captured fin rays of the micro-CT generated model. When using a CFD program, it is convenient to label geometry to make it easier to run the simulation. Figure 3.3 below shows the fluid volume around the cross-section of the fish and 3 labeled geometries: 2 faces and 1 body. This process allows us to run the simulation around a cross-section cutout of the micro-CT reconstruction of the fish.

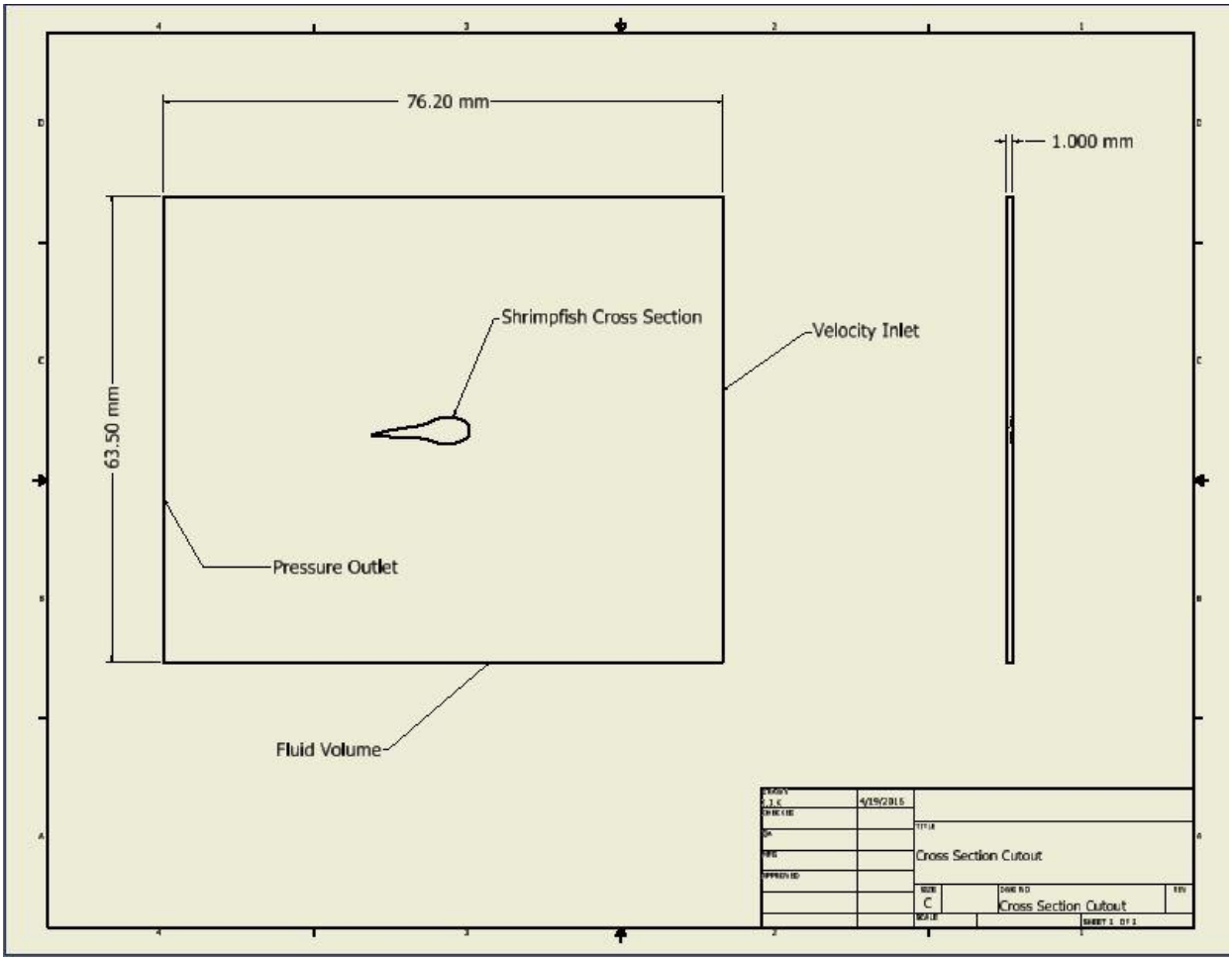

Figure 3.3: Shrimpfish cross-section cutout, see text for details.

The above geometry was imported into Ansys workbench and the displayed surfaces and volume were labeled. The velocity inlet indicates the face at which the velocity of the fluid surrounding *Aeoliscus* is set. The pressure outlet indicates the face at which the fluid exits the simulation. The pressure is set to 0 to ensure there is no back pressure obscuring the flow from exiting the simulation. The next step involves setting mesh parameters, building the mesh and ensuring that the quality of the mesh is satisfactory. To ensure a quality mesh was built, a specific size was chosen 6 e^{-4} m. This size allows for adequate resolution around the external surface of the shrimpfish cross-section. The shape of the mesh element chosen was tetrahedron as it offers better solution results despite taking longer to solve. After the mesh was built the quality has to be examined. The mesh that was built composed of 394337

elements and a minimum orthogonal quality of 0.01 which Ansys confirms as acceptable. The orthogonal quality of a cell is the minimum value that results from calculating the normalized dot product of the area vector of a face and a vector from the centroid of the cell to the centroid of that face and the normalized dot product of the area vector of a face and a vector from the centroid of the cell to the centroid of the adjacent cell that shares that face. Therefore, the worst cells will have an orthogonal quality closer to 0 and the best cells will have an orthogonal quality closer to 1. [14]

To solve the flow around *Aeoliscus* the laminar flow model, as dictated by the Reynolds number, was chosen. For laminar flow Fluent solves the Navier-Stokes equations using the finite volume method. As with any solver some initial conditions must be set. For the flow input the maximum observed velocity at the input was used, 300 mm/s with an outlet pressure of zero ensuring that the flow will not be obstructed after it passes over the cross-section. It should be noted that the same fish that displayed the maximum observed velocity was not used to create the cross-section cutout used in the flow simulation. Due to complications in the micro-CT process, the fish was unavailable so a fish of similar size was used. The dynamic viscosity and density of the fluid was set to that used in the Reynolds number calculation, 0.980×10^{-3} kg/m*s and 1023.34 kg/m^3 respectively. Once all initial conditions were set, the solution was run for 1000 iterations. To examine the quality of the solution, we have to examine the change in each of the terms in the mathematical model as the solution iterates. If the terms do not converge, the solution is regarded as inaccurate. Convergence of continuity and all three component velocities occurred around 350 iterations; figure 3.4 below shows the convergence.

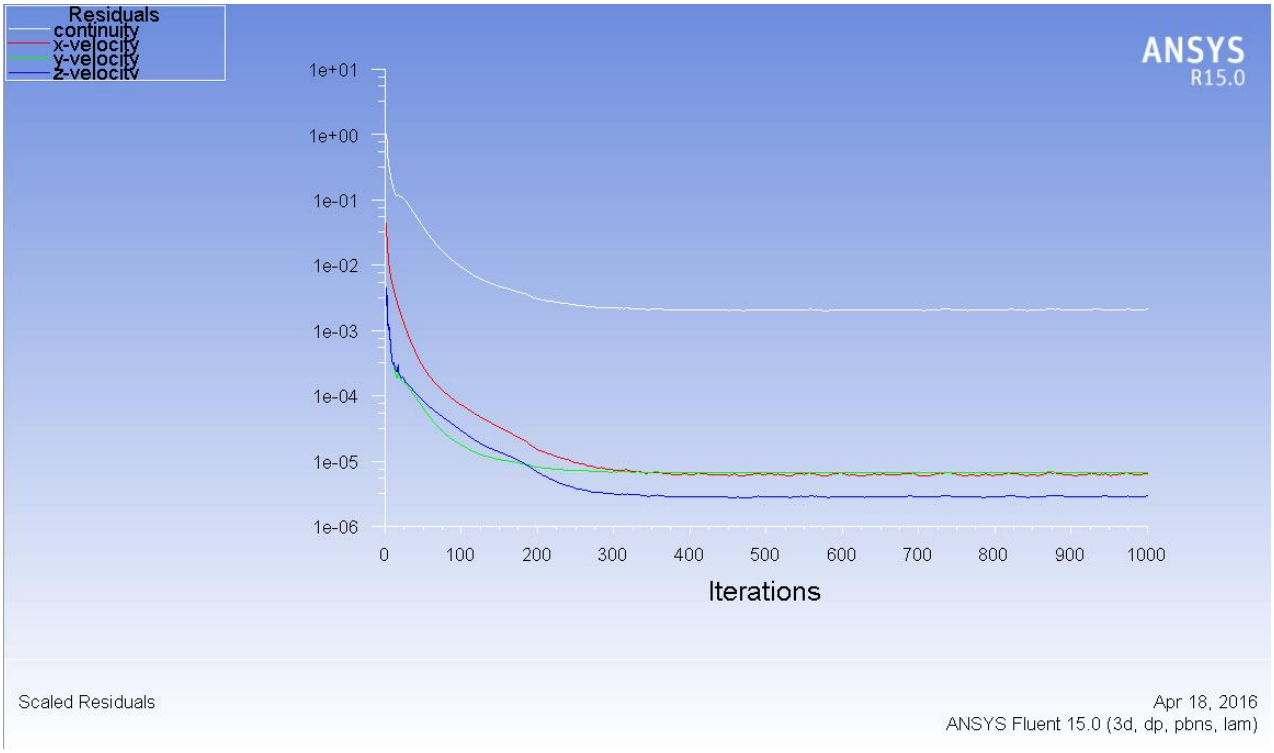

Figure 3.4: Convergence of computational residuals. Iteration vs change in term value.

Post processing in Fluent allows for various contours plots, vector plots and force calculations; for our research we required the coefficient of drag. Ansys provides a method to calculate the coefficient of drag, providing for both the pressure and viscous effects. To compliment the C_D calculation a static pressure contour and velocity vector plot were created. Figure 3.5 shows the static pressure contour while figure 3.6 shows the velocity vectors encompassing *Aeoliscus's* cross-section. The highest observed pressure, encompassed by the circle shown in figure 3.5, was located on the leading edge of the fish and was just shy of 230 Pascal. The largest velocity observed, roughly 55 cm/s, was along the edges of the profile where the pressure was the lowest.

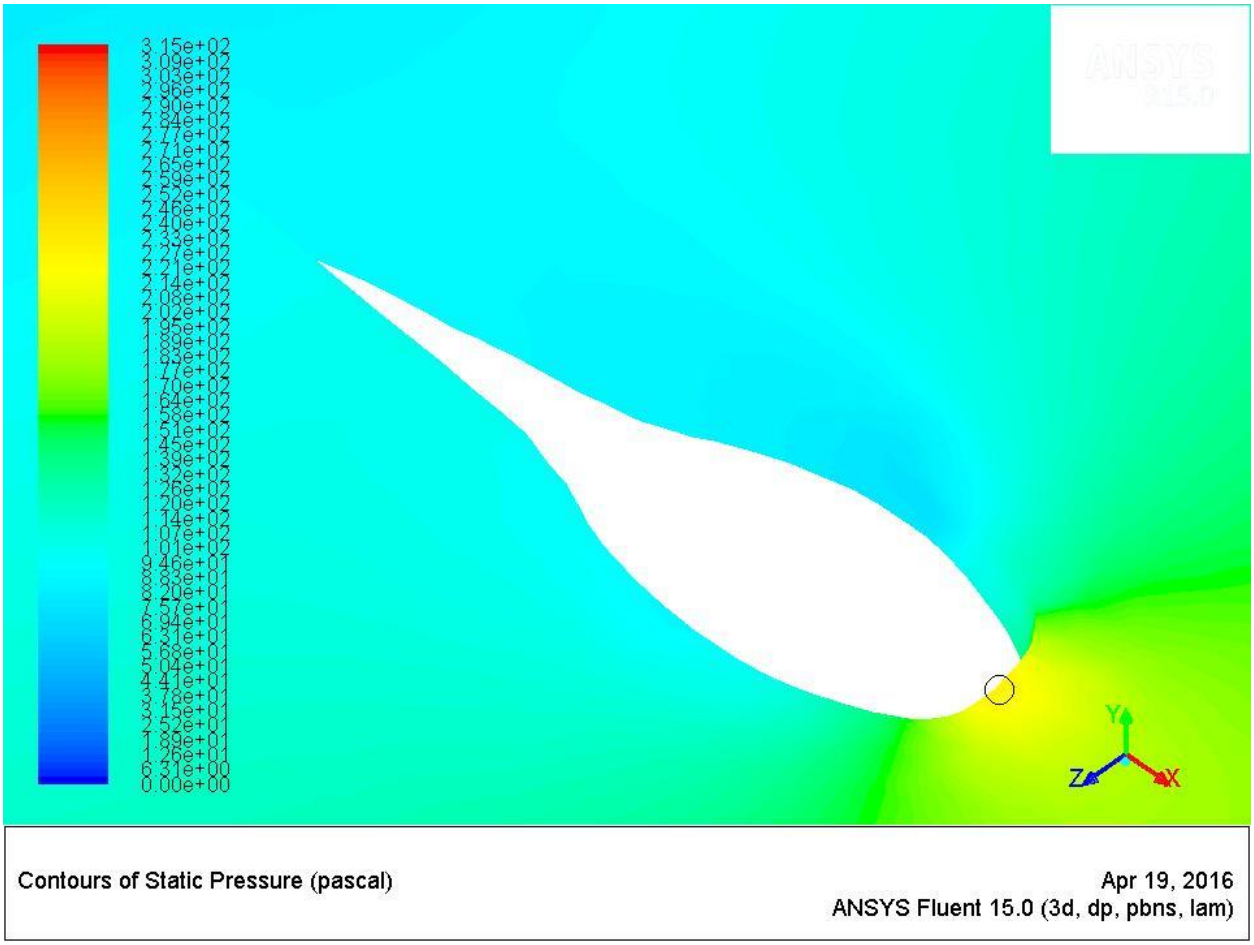

Figure 3.5: Contours of static pressure.

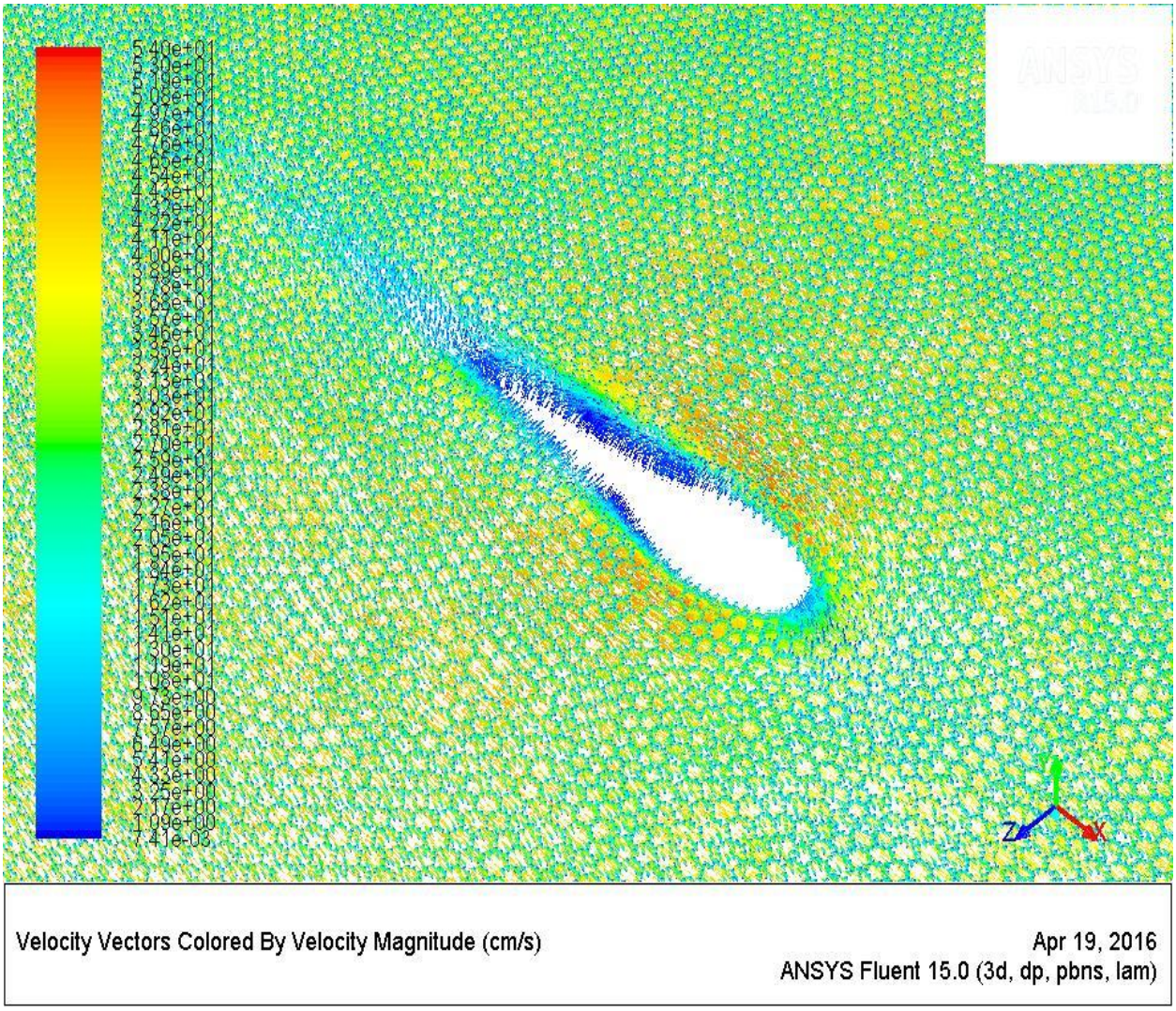

Figure 3.6: Velocity vector magnitude plot

Finally the C_D was gathered from Ansys with a value of 0.03.

Chapter 4: Discussion

Stability and maneuverability are inversely correlated; the more stable a body is, the more force it takes to move that body. Body structures that have evolved to provide stable movements are not adaptable to provide high maneuverability. Fish that are more stable than others need to expend less energy to station hold and travel long distances but do not have the control to maneuver in complex environments. [4] Rapid and complex maneuvers are energetically expensive since the fish has to expend energy for the desired movement along with countering the stabilizing forces. With *Aeoliscus*, the gravitational force coupled with the CG and the buoyant force coupled with the CB are the two factors that influence the stability around the pitch axis. Figure 4.1 below shows the axis breakdown. We discovered that the gravitational force was greater but, on average, was less than 7 % greater than the buoyant force proving *Aeoliscus* to be negatively buoyant. To complete our examination of stability and determine the location of the CG and CB were determined. Our methods yielded a distance between the CG and CB of roughly 1.0% that of the standard length. This leaves *Aeoliscus* extremely sensitive to outside forces but also allows *Aeoliscus* to exert very little force to execute desired motion. This is the characteristic of a highly maneuverable fish.

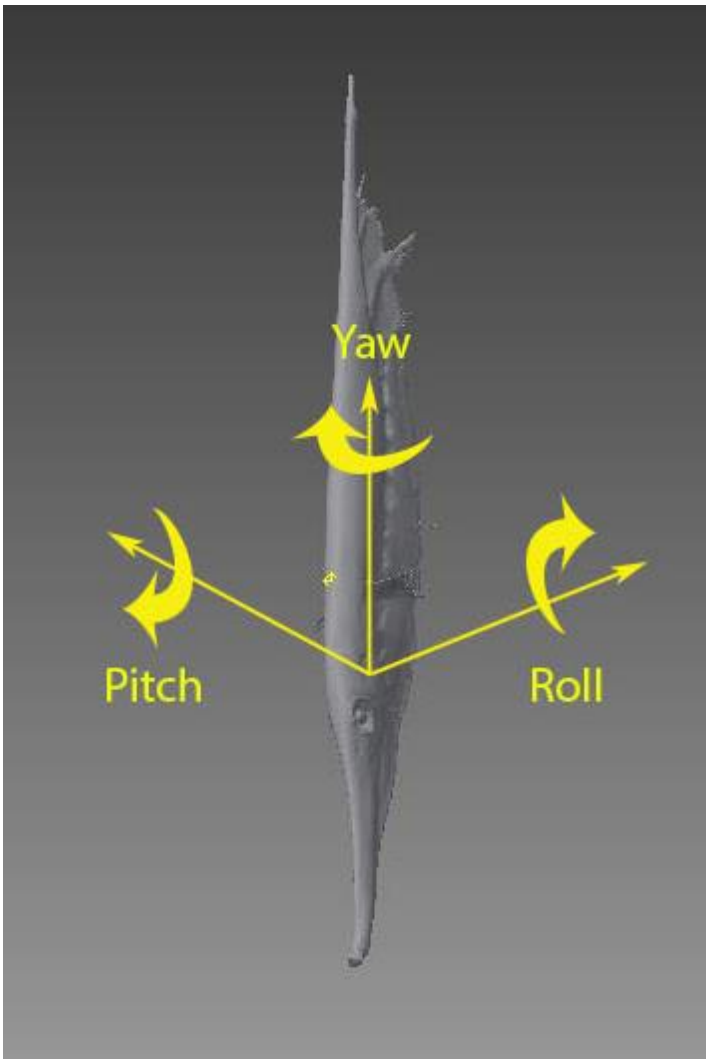

Figure 4.1: Micro-CT generated 3D model with labeled axes.

Our results showed discrepancies between the two methods of determining the CB. While the A-P normalization revealed a 1% difference between the micro-CT produced results and the experimental results, there was an 8% D-V difference between the methods. Surface tension is commonly calculated in units of force/length. While convenient this calculation only takes into account the intrinsic properties of the fluid and not the area over which the tensions occurs. To calculate the force due to interfacial tension, you must know the area over which the force is acting. When partially submerging *Aeoliscus* during experimental CB testing, 3 different angles were used. The angles were not measured or set to distinct values. These varying angles may have caused a different amount of surface area to be exposed to the effects of surface tension. As the interfacial tension force is dependent on area, I believe this was the source for most of the discrepancy between these two varying results.

Live shrimpfish often swim at an angle from the vertical and, when swimming fact assume a horizontal posture. They always, however, seem to "relax" into a vertical orientation after a bout of swimming. This "relaxation" caused us to hypothesize that Aeoliscus is hydrostatically stable, which is clearly not the case as shown from our measurements. Interestingly if a euthanized *Aeoliscus* was dropped into a beaker filled with still water, it will orient itself into a perfectly vertical posture and balance on its snout until disturbed by an outside force. Figures 4.2 and 4.3 below show a dead *Aeoliscus* balanced on the tip of its snout in an aquarium. An unstable body, with the CG above the CB will either flip over or in stay in its original orientation if the CG is placed exactly above the CB. At this equilibrium position the weight and the buoyant forces cancel each other and there is no turning moment. In a simple elongate shape this equilibrium point requires careful orientation of the body and, of course, no perturbing currents. The shrimpfish, however, seem to readily assume the equilibrium position in the absence of currents. Perhaps the shape of the body generates hydrodynamic forces as it moves downward (it is negatively buoyant) to drive the body into the equilibrium position. This would be an interesting hypothesis to test in future experiments.

Figure 4.2: Side view of *Aeoliscus* balancing on its snout.

Figure 4.3: Front view of *Aeoliscus* balancing on its snout.

Maneuverability was examined next. To quantify maneuverability we adopted the same dimension that was utilized by Webb [13], the turning radius. Observing and recording *Aeoliscus* from above revealed that *Aeoliscus* could turn on an axis that resides within its body, giving a turning radius of 0. This confirmed our suspicion that the fish is highly maneuverable. Values for maneuverability for a variety of fish are given below, note that a maneuverability of 0 means the fish turns on axis. [13]

1. Yellowtail (*Seriola dorsalis*): 0.23
2. Rainbow trout (*Oncorhynchus mykiss*): 0.18
3. Dolphin(*Coryphaena hippurus*): 0.13
4. Small mouth bass (*Micropterus dolomieu*): 0.11
5. Angelfish (*Pterophyllum eimekei*): 0.065
6. Seahorses (multiple species): 0

In comparison to the other fish listed, only the seahorse shared the 0 turning radius with *Aeoliscus*. The seahorse is also the only fish that utilizes the same swimming technique, median paired fin propulsion, and the head down vertical posture and rigid body.

Finally the coefficient of drag was determined. The velocity was determined and showed that the shrimpfish can swim at over 22 body lengths per second. Using the velocity and the characteristic length, the associated Reynolds number, 4222, revealed that the flow around *Aeoliscus* was laminar. Using Inventor the profile of *Aeoliscus* was inserted into a fluid control volume and Ansys was used to simulate a laminar external flow. Ansys calculated a coefficient of drag of 0.029 which is less than that of a streamlined airfoil.

A more useful comparison is between *Aeoliscus* and other fish. The drag coefficient of the seahorse, whose body is not streamlined like *Aeoliscus*, is on the order of 10^{-1} while the streamlined body of the angelfish has a drag coefficient closer to the order of 10^{-2}. [15] Webb examined the drag coefficients and Reynolds number at varying velocities for *Oncorhynchus kisutch* and *Salmo gairdneri* using dead-drag

measurements in a water tunnel. [16] To give an idea of size, *Oncorhynchus kisutch* weighed 2217 grams while 2 *Salmo gairdneris* were measured, 254 grams and 278 grams. Webb found that at roughly 30 cm/s, *Salmo* had a Reynolds number that remained in the realm of laminar flow. Once 40 cm/s was reached, the flow began to transition into turbulent but the coefficient of drag showed little change, 0.022 and 0.019 respectively. *Oncorhynchus kisutch's* velocity ranged from 20 cm/s to 90 cm/s and the coefficient of drag ranged from 0.026 to 0.018 respectively with a Reynolds number in the transition between laminar ant turbulent flow.

Measurement of drag by towing a dead fish is problematic because most fish have flexible bodies that deform while they move thus changing the drag force over the course of a swimming cycle. The drag determined from a dead, non-moving fish may be of little value in understanding the hydrodynamics of a swimming fish [15]. Aeoliscus, however, has a rigid body that does not flex while swimming so measurements of drag on a stationary shrimpfish, or a model of one, is relevant to the fish in the living state.

Overall, *Aeoliscus* is a slightly unstable, highly maneuverable fish whose streamlined body produces little turbulence in the surrounding fluid. A low coefficient of drag proves its body moves through water efficiently. This makes it a good candidate to serve as the basis for a biomimetic AUV.

References

[1] Merriam-Webster, 2016.

[2] R. H. Kuiter, Seahorses, Pipefishes and their relatives, Chorlywood, UK: TMC Publishing, 2003.

[3] C. E. Bond, Biology of Fishes, 2nd ed., Saunders College Publishing, 1996.

[4] D. Weihs, "Stability of Aquatic Locomotion," in *Fluid Dynamics in Biology*, Contemporary Mathematics, 1993.

[5] A. Biran, Ship Hydrostatics and Stability, 2003.

[6] F. White, Fluid Mechanics, 7th ed., McGraw-Hill, 2008.

[7] M. Plesha, G. Gray and F. Costanzo, Engineering Mechanics: Statics, 2nd ed., McGraw-Hill, 2013.

[8] D. Kleppner and R. Kolenkow, An Introduction to Mechanics, 2nd ed., Cambridge University Press, 2014.

[9] R. S. Stock, MicroComputed Tomography: Methodology and Applications, 2009.

[10] Carl Zeiss X-Ray Microscopy, Zeiss Xradia 410 Vera.

[11] Y. Liu, F. Meirer, P. A. Williams, J. Wang, J. C. Andrews and P. Pianetta, "TXM-Wizard: a program for advanced data collection and evaluation in full-field transmission X-ray microscopy".

[12] U. M. Norberg and J. M. Rayner, "Ecological Morphology and Flight in Bats (Mammalia; Chiroptera): Wing Adaptations, Flight Performance, Foraging Strategy and Echolocation," in *Philisophical Transactions of the Royal Society of London B*, vol. 316, 1987, pp. 335-427.

[13] P. Webb, "The Biology of Fish Swimming," in *Mechanics and Physiology of Animal Swimmin*, 1994, pp. 45-62.

[14] Ansys, Inc, Ansys Help, 2013.

[15] R. W. Blake, Fish Locomotion, Cambridge University Press, 1983.

[16] P. W. Webb, "Hydrodynamics and Energetics of Fish Propulsion," Department of the Environment Fisheries and Marine Service, 1975.

Appendix A: CG and CB Overlays

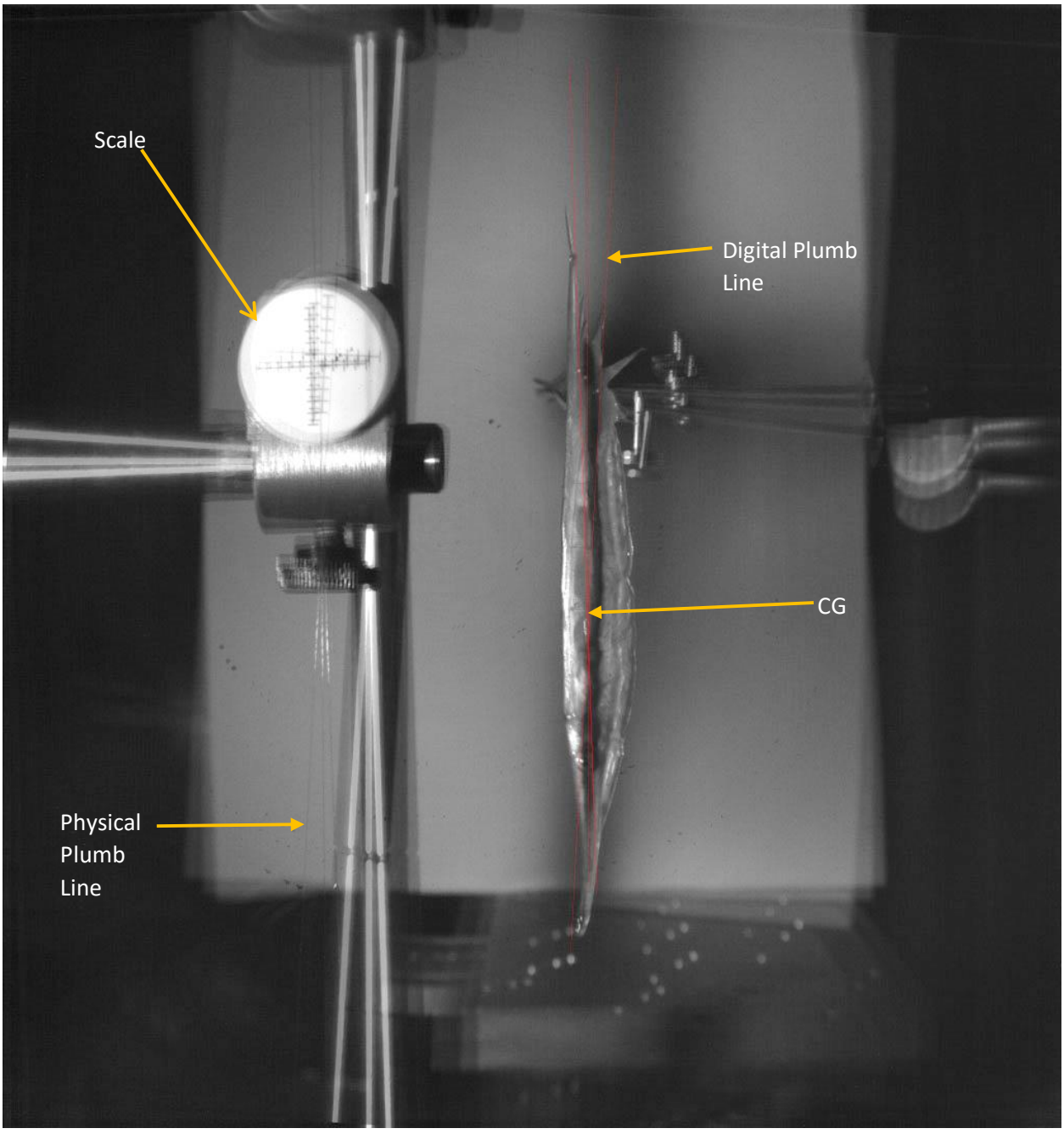

Figure A.1: Fish 7 CG Overlay

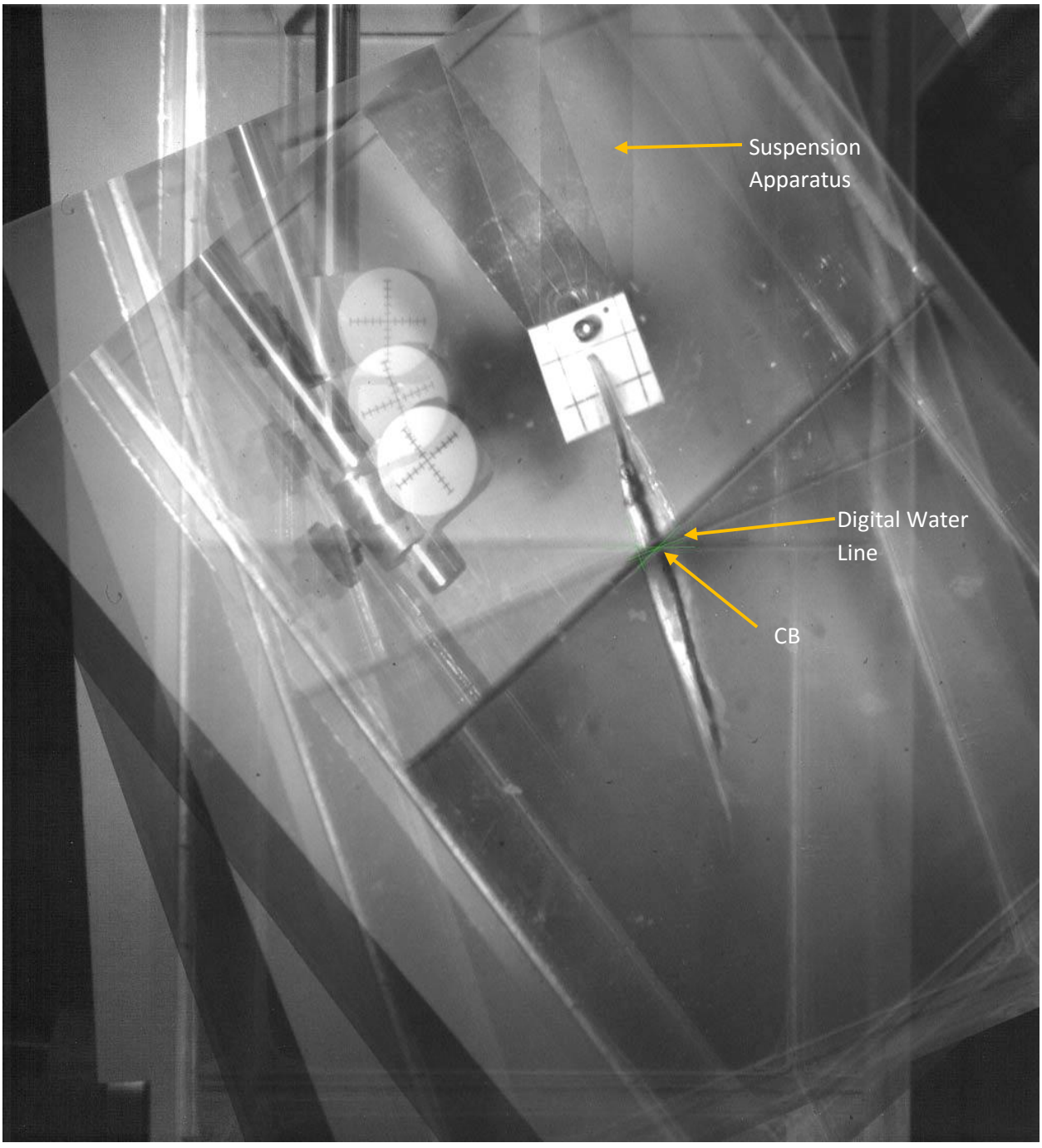

Figure A.2: Fish 7 CB Overlay

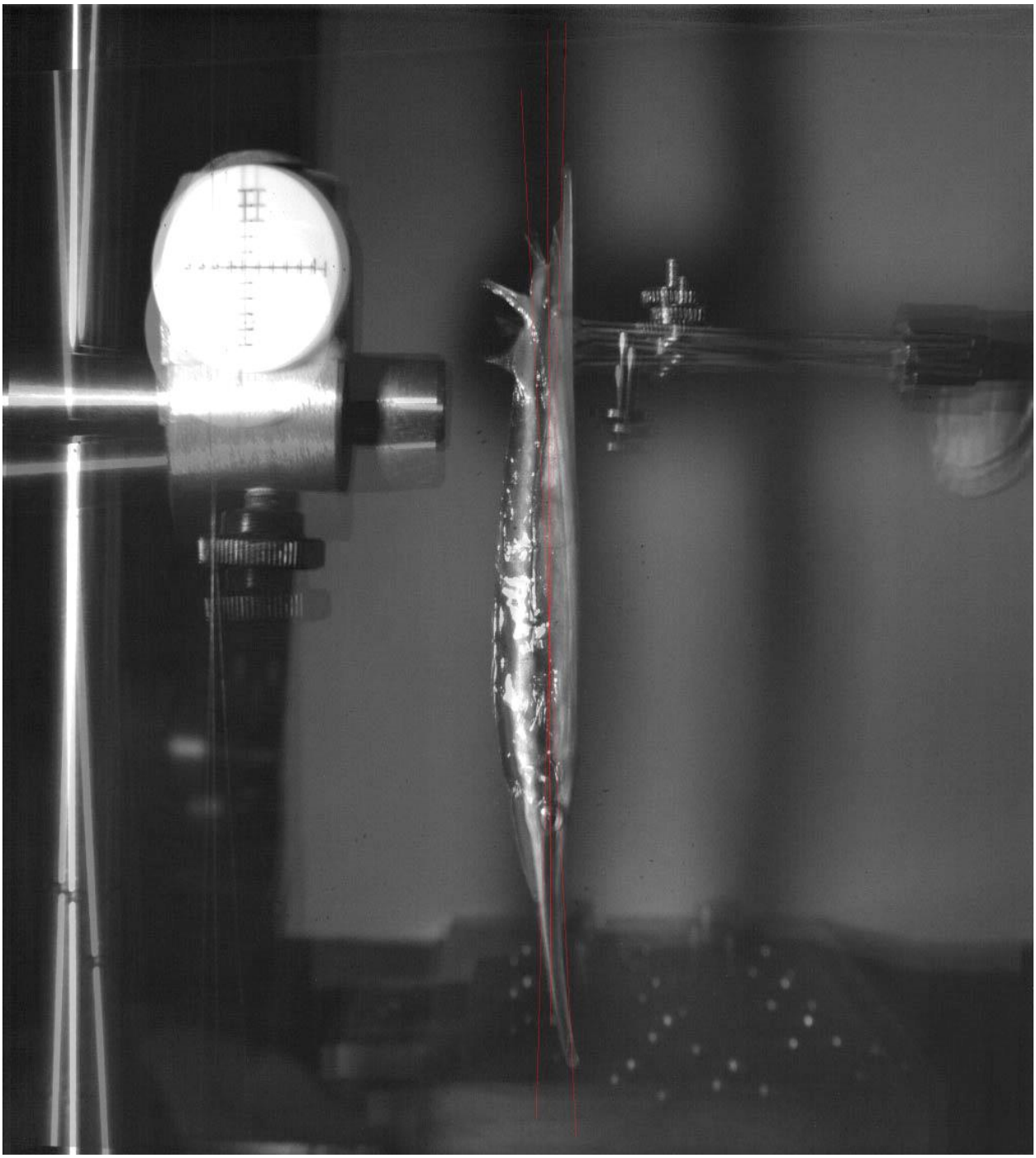

Figure A.3: Fish 8 CG Overlay

Figure A.4: Fish 8 CB Overlay

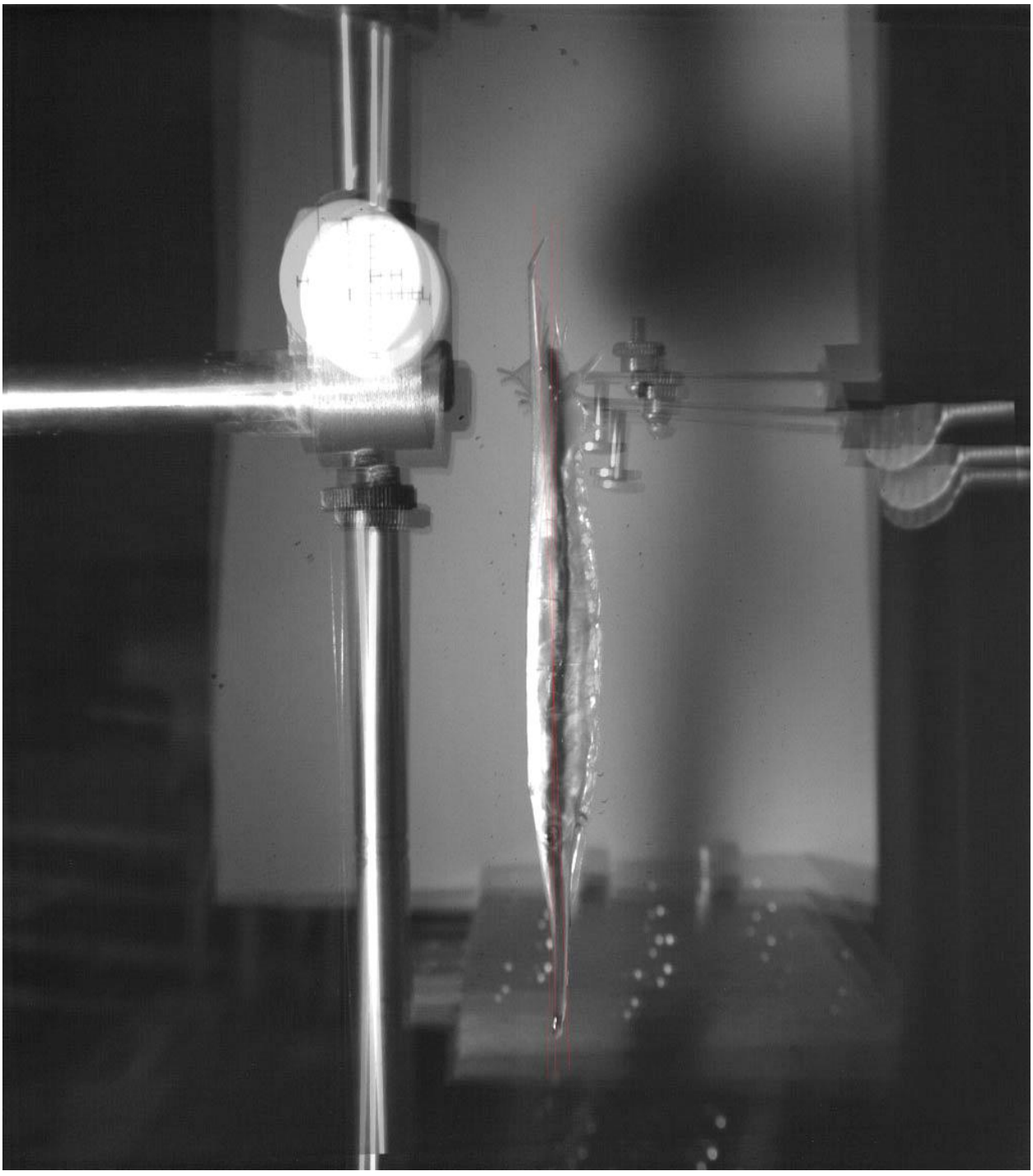

Figure A.5: Fish 9 CG Overlay

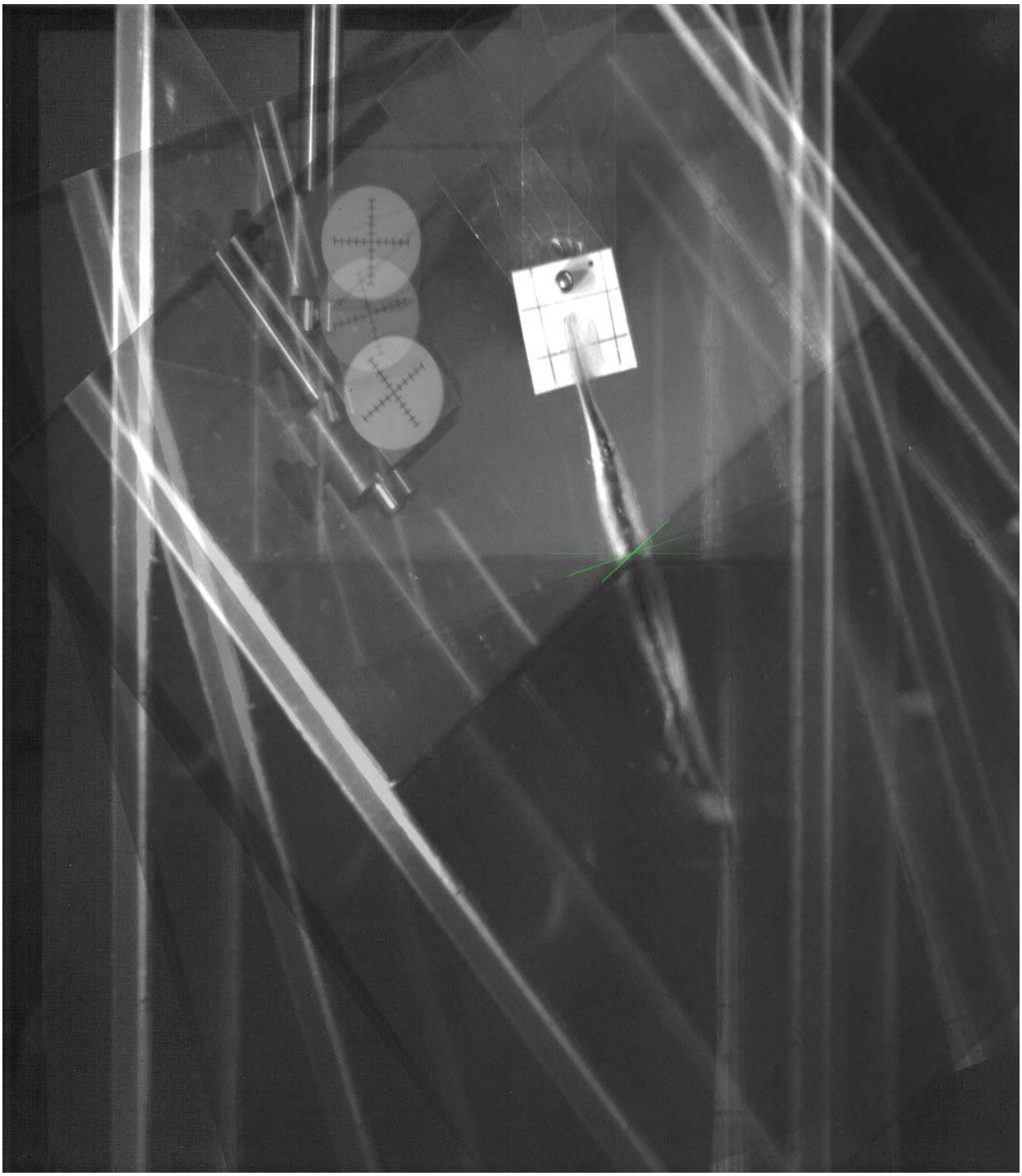

Figure A.6: Fish 9 CB Overlay

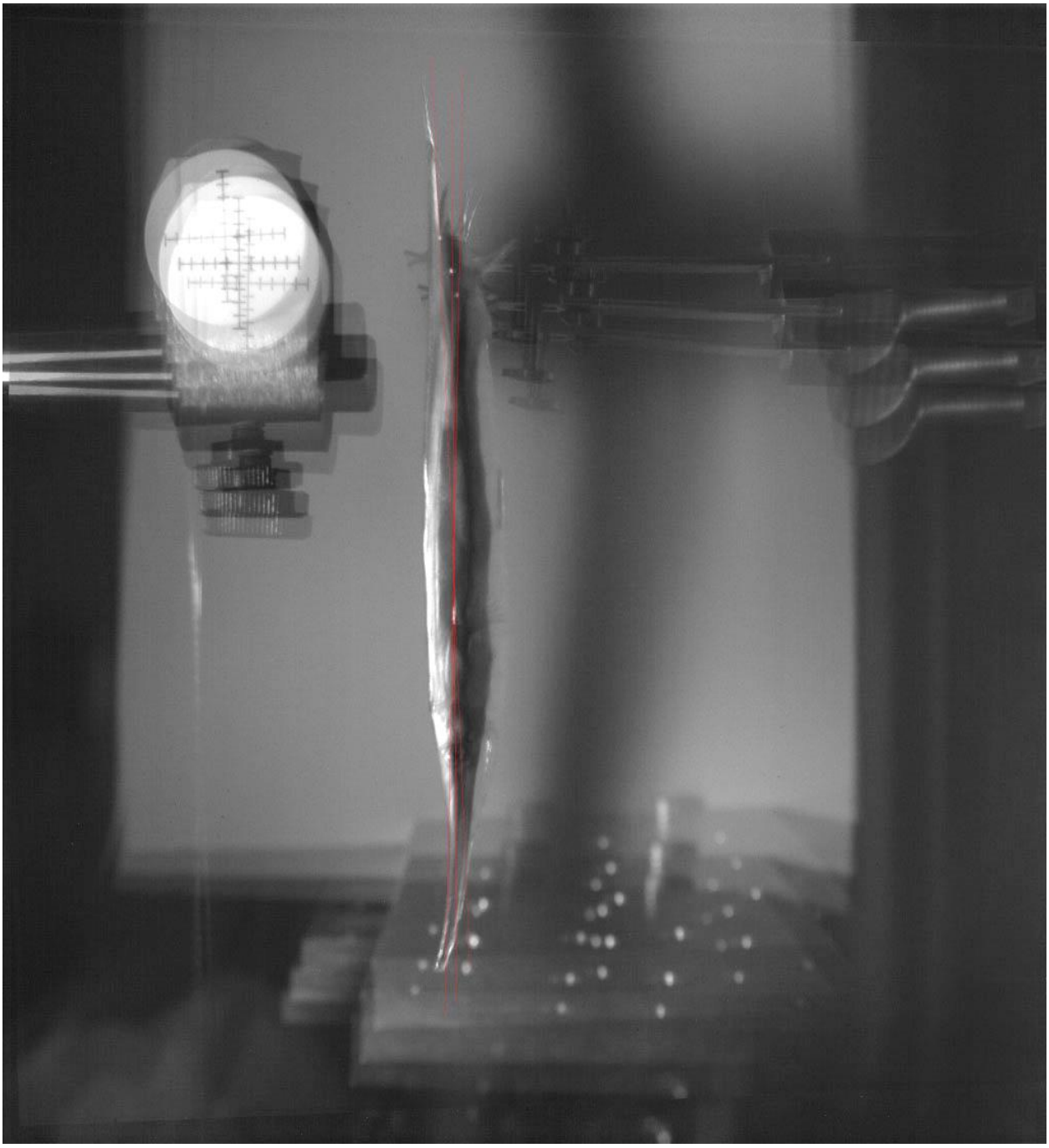

Figure A.7: Fish 10 CG Overlay

Figure A.8: Fish 10 CB Overlay

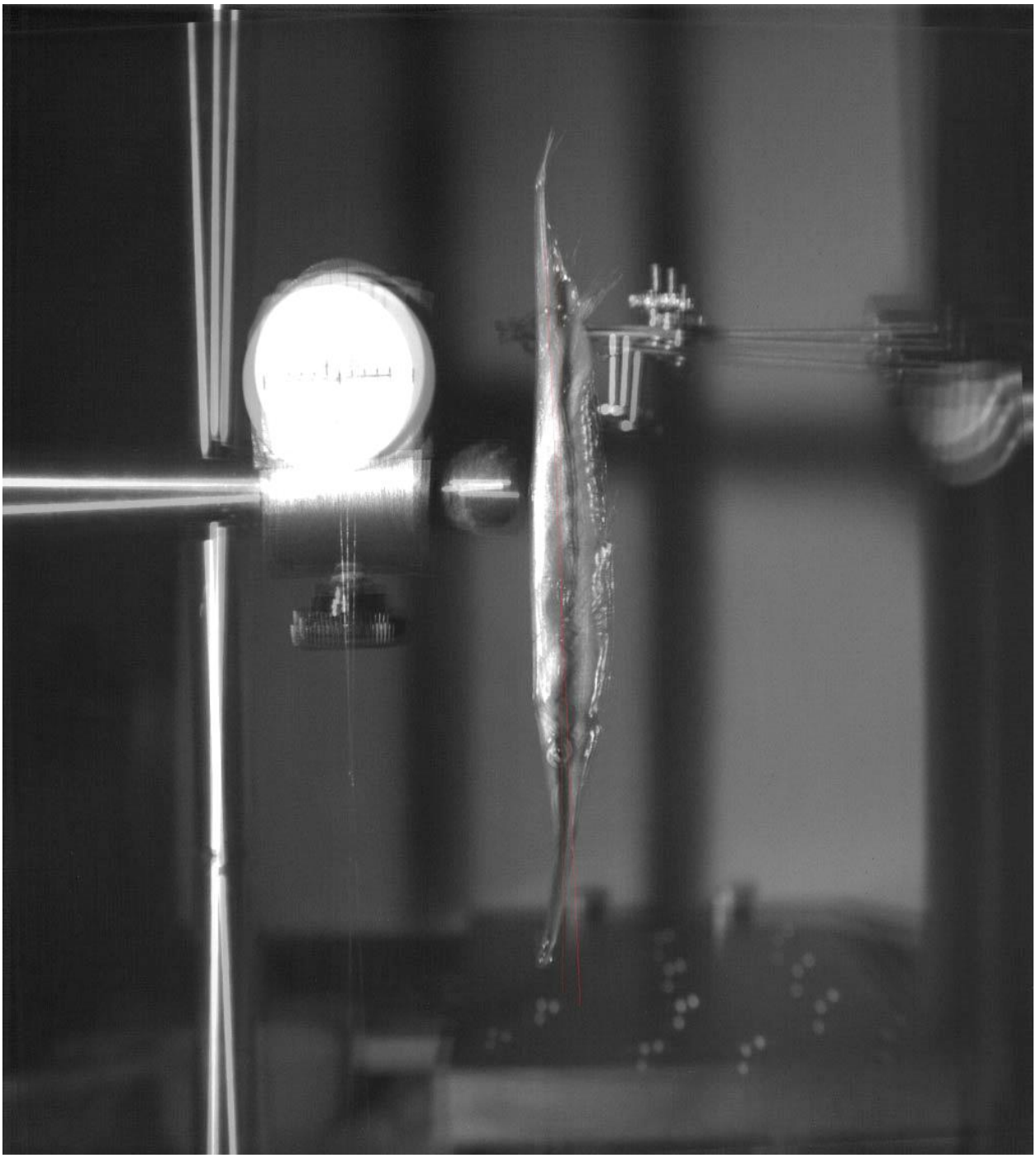

Figure A.9: Fish 11 CG Overlay

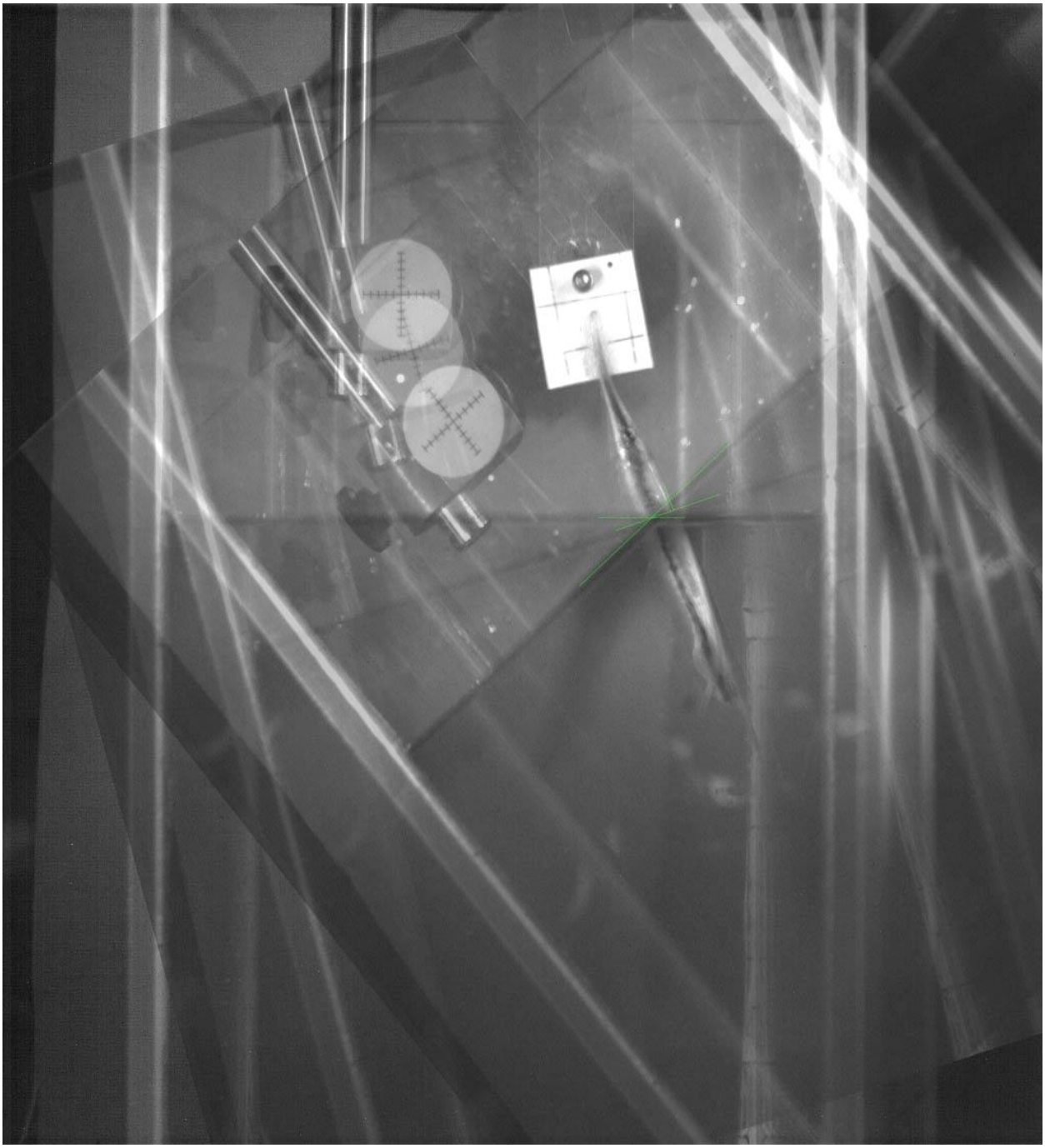

Figure A.10: Fish 11 CB Overlay

Appendix B: Control Stick Overlays

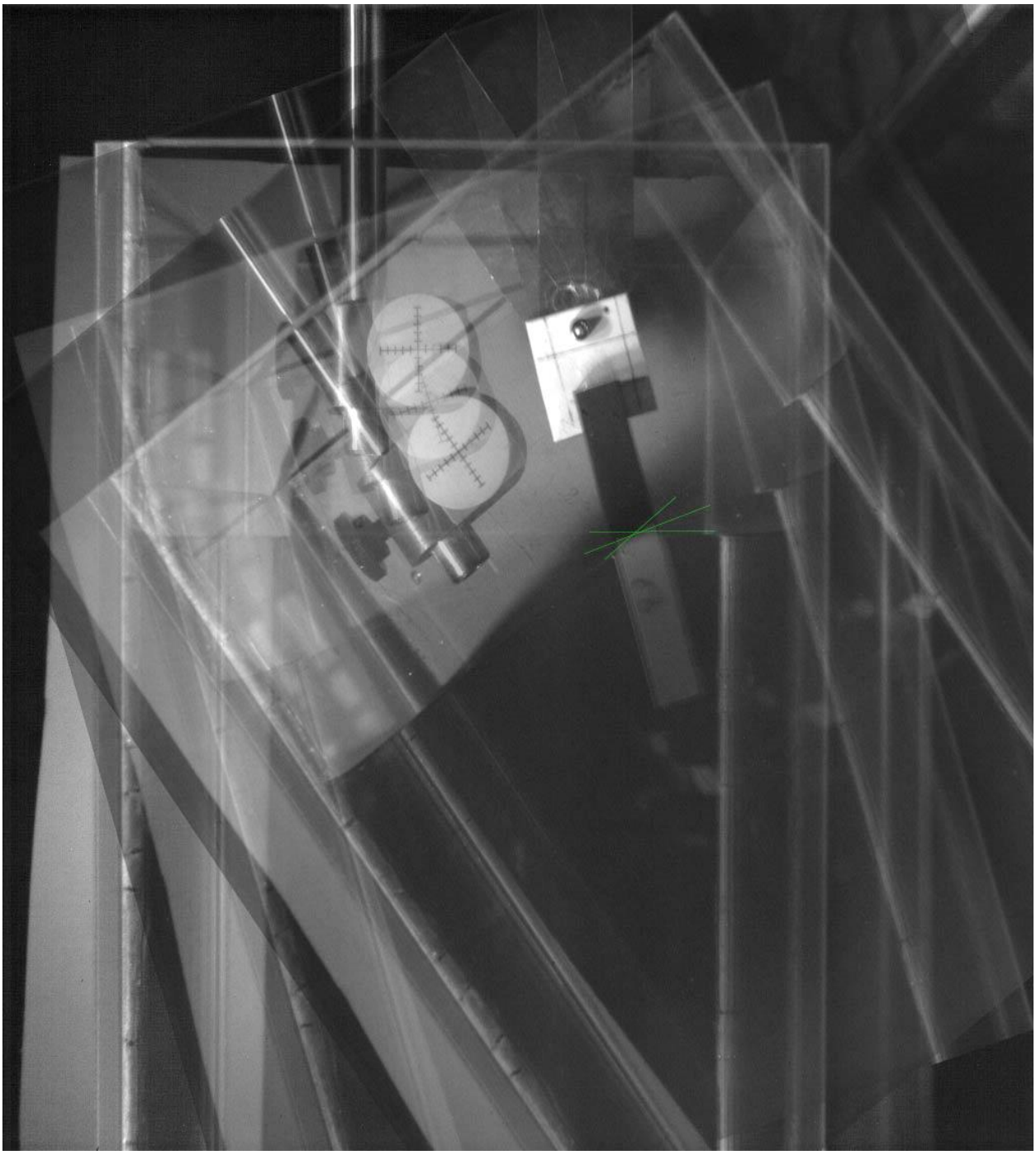

Figure B.1: Control stick CB overlay without surfactant.

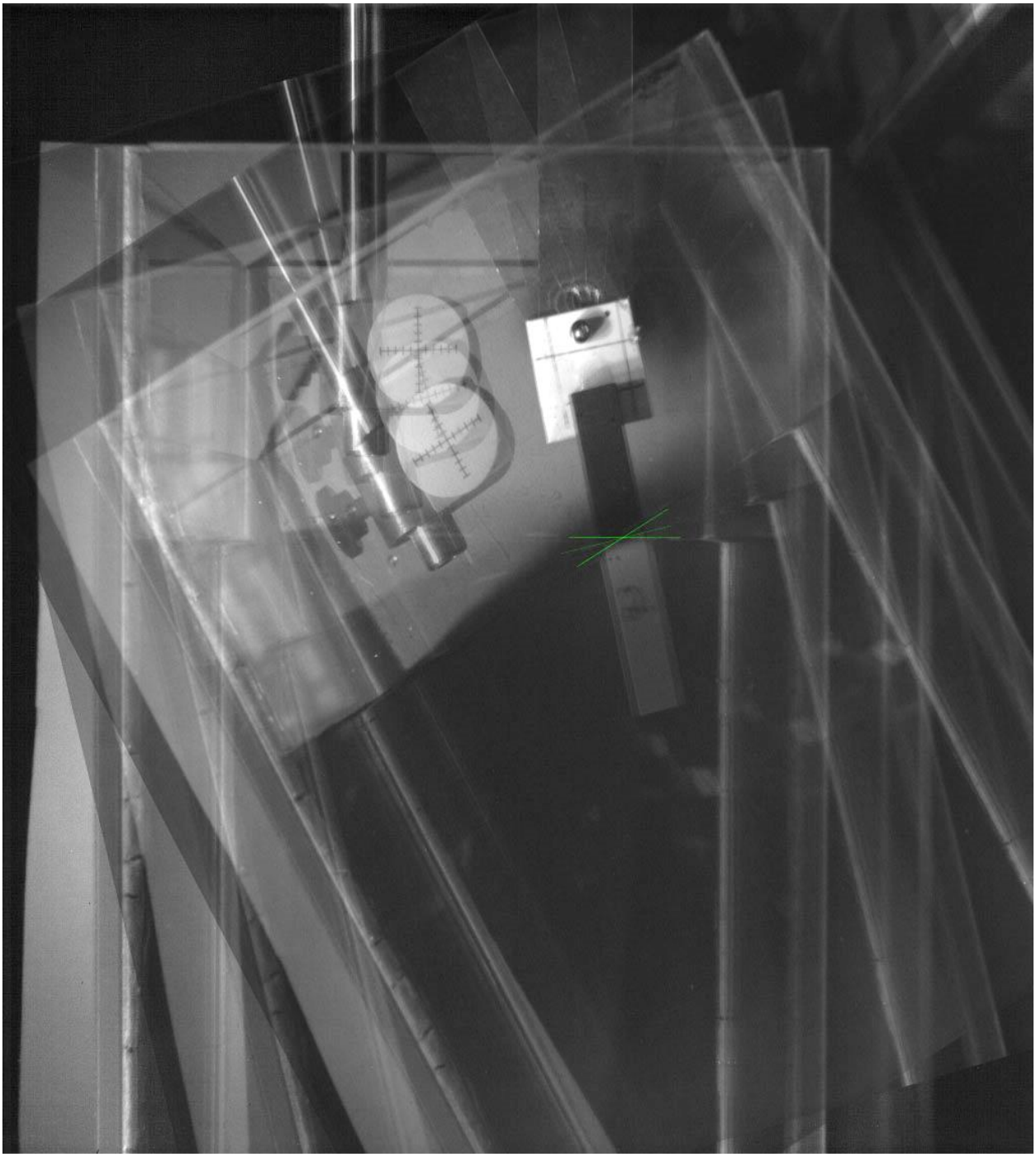

Figure B.2: Control Stick CB overlay with surfactant.

Appendix C: Velocity Analysis Matlab Script

```
function [ Velocity ] = Velocity( C, R, FileName )
% This program takes an input array of x and y coordinates (C) and given
frame rate (R) and computes the x/y velocity components and overall
% magnitude and direction.It saves the data in a text file title
% "FileName".

n = size(C,1); %grabs number of rows in array C
deltaT = 1/R; %calculate the change in time for each row of C
X = C(1,1)-C(1,1); %Set initial x to zero
Y = C(1,2)-C(1,2); %Set initial y to zero
Ti = deltaT;
time = 0;
Vx = [];
Vy = [];
V = [];
z=1;



for i=2:n
  Xi = C(i,1)-C(1,1); %Frame by frame change in X position
  X = [X; Xi]; %Add frame by frame change in X to column vector
  Yi = C(i,2)-C(1,2); %Frame by frame change in Y position
  Y = [Y; Yi]; %Add frame by frame change in Y to column vector
  Ti = Ti + deltaT; %Increment time
  time = [time; Ti]; %Add frame by frame change in time to column vector


  if(i == R/4*z)%checks to see if 1/4 second has passed
    Vxi = Xi/Ti; %Frame by frame x velocity for first frame
    Vx = [Vx; Vxi];
    Vyi = Yi/Ti; %Frame by frame y velocity for first frame
    Vy = [Vy; Vyi];
    Vi = (Vxi^2+Vyi^2)^(1/2); %Total velocity magnitude.
    V = [V; Vi];
    z = z+1; %increments z for time test
  end

end

MaxVelocity = max(V); %Pulls the maximum value from V
fileID = fopen(FileName,'w');
fprintf(fileID,  'Max veolcity: \n');
fprintf(fileID, '%f %f \n',MaxVelocity); %:creates a text file of the maximum
velocty
fclose (fileID);

figure;
plot(time, Y)
title('Y Position vs Time');
xlabel('Time (s)');
ylabel('Y Position (mm)');

figure;
```

```
plot(time, X)
title('X Position vs Time');
xlabel('Time (s)');
ylabel('X Position (mm)');
```